Groundwater affects the geomorphic and hydrologic properties of coevolved landscapes

David G. Litwin[1], Gregory E. Tucker[2,3], Katherine R. Barnhart[2,3,4], Ciaran J. Harman[1,5]

[1]Deptartment of Environmental Health and Engineering, Johns Hopkins University, Baltimore, MD, USA
[2]Cooperative Institute for Research in Environmental Sciences (CIRES), University of Colorado, Boulder, CO, USA
[3]Department of Geological Sciences, University of Colorado, Boulder, CO, USA
[4]Now at U.S. Geological Survey, Landslide Hazards Program, Golden, CO, USA
[1]Deptartment of Earth and Planetary Science, Johns Hopkins University, Baltimore, MD, USA

Key Points:

- Presents a coupled model of shallow groundwater and landscape evolution to examine coevolution of runoff generation and landscape morphology
- Analysis of the model suggest that hillslope length scales nonlinearly with subsurface drainage capacity relative to the recharge rate
- Emergent morphology can be characterized by 3 metrics (steepness, curvature, topographic index) and is controlled by 3 dimensionless numbers

Corresponding author: Ciaran J. Harman, `charman1@jhu.edu`

Abstract

The hydrologic dynamics and geomorphic evolution of watersheds are intimately coupled – runoff generation and water storage are controlled by topography and properties of the surface and subsurface, while also affecting the evolution of those properties over geologic time. However, the large disparity between their timescales has made it difficult to examine interdependent controls on emergent hydro-geomorphic properties, such as hillslope length, drainage density, extent of surface saturation. In this study, we develop a new model coupling hydrology and landscape evolution to explore how runoff generation affects long-term catchment evolution, and analyze numerical results using a nondimensional scaling framework. We focus on hydrologic processes dominating in humid climates where storm runoff primarily arises from shallow subsurface flow and from precipitation on saturated areas. The model solves hydraulic groundwater equations to predict the water table location given prescribed, constant groundwater recharge. Water in excess of the subsurface capacity for transport becomes overland flow, which generates shear stress on the surface and may detach and transport sediment. This affects the landscape form that in turn affects runoff generation. We show that (1) three dimensionless parameters describe the possible steady state landscapes that coevolve under steady recharge; (2) hillslope length increases with increasing transmissivity relative to the recharge rate; (3) three topographic metrics—steepness index, Laplacian curvature, and topographic index—provide a basis to recover key model parameters from topography (including subsurface transmissivity). These results open possibilities for topographic analysis of humid upland landscapes that could inform quantitative understanding of hydrological processes at the landscape scale.

1 Introduction

1.1 Motivation

Landscape morphology and subsurface structure are strong predictors of runoff generation style and spatial distribution (Dunne, 1978). In humid climates, the infiltration capacity of undisturbed soil is high and overland flow due to exceedance of soil infiltration capacity is rare. When relief is relatively low and soils are relatively thin, runoff is most commonly generated by the expansion of variable source areas, which may generate overland flow where precipitation falls directly on saturated areas (Dunne & Black, 1970). In steeper landscapes with deep soils, water may be transmitted laterally through the subsurface at permeability contrasts, becoming surface runoff only when it reaches stream channels (Hewlett & Hibbert, 1967). Saturated areas (including wetted stream channels) emerge as the supply of water from upslope areas exceeds the conveyance capacity of water through the subsurface. This competition between upslope supply and downslope transport capacity links properties of the subsurface, such as transmissivity, to the runoff response of watersheds as a whole (O'Loughlin, 1981). Furthermore, overland flow generates shear stress on the land surface that may detach and transport sediment. This drives the evolution of topographic convergence/divergence and convexity/concavity, which are important controls on runoff generation themselves (Prancevic & Kirchner, 2019; Troch et al., 2003; Lapides et al., 2020).

Research also suggests that incision and hillslope sediment transport play a role in setting the rate and extent of subsurface weathering by setting the rate at which fresh bedrock is supplied to the near surface (Gabet & Mudd, 2009; West et al., 2005). Subsurface weathering is in turn crucial for setting subsurface properties that affect groundwater flow and storage capacity. These feedbacks suggest that there should be intimate links between runoff generation behavior and landscape morphology. If morphology affects and is affected by runoff generation, how might long-term evolution set the extent of surface saturation in a landscape? Are there emergent relationships between topographic

form and shallow subsurface hydrology that we could quantify? Here we will draw insights from coupled a coupled hydro-geomorphic model to answer these questions.

1.2 Background

Over geologic time, upland landscapes are shaped by the competition between incision by overland flow, gravitationally-driven fluxes of sediment due to processes including biogenic disturbance and frost heaving, and baselevel change (Howard, 1994). While it is not possible to observe the evolution of landscapes at human timescales, numerical landscape evolution models (LEMs) have allowed researchers to make substantial progress in understanding how landscapes respond to dynamic forcings of tectonics, lithology, and climate (e.g., reviews by Chen et al., 2014; Bishop, 2007; Martin & Church, 2004; Pelletier, 2013; Pazzaglia, 2003; Temme et al., 2013; Valters, 2016). However, the treatment of hydrology in models that consider evolution over geologic time remains rudimentary.

Early LEMs treated runoff as the product of upslope area and an effective precipitation rate (Willgoose, Bras, & Rodriguez-Iturbe, 1991; Ahnert, 1976; Armstrong, 1976), representing the time-averaged runoff from infiltration excess overland flow. In these models, all areas of the landscape generated surface runoff simultaneously, though all areas may not experience erosion due to the presence of thresholds for sediment detachment (Horton, 1945). The practice of using such runoff formulations in LEMs is still common today when hydrologic response is not central to the study, as models with minimal hydrologic dynamics can still effectively capture certain essential aspects of landscape form (e.g., Forte et al., 2016; Barnhart, Tucker, Doty, Glade, et al., 2020; Theodoratos et al., 2018). One of the first attempts to capture subsurface hydrology in a LEM came when Ijjász-Vásquez et al. (1992) developed a model that partitioned flow between surface and subsurface using a steady state topographic index criterion (Beven & Kirkby, 1979). The authors found that this partitioning significantly changed catchment hypsometry in comparison to the infiltration excess formulation. Tucker and Bras (1998) compared several different landscape evolution and runoff generation formulations, including one that treats subsurface transport capacity similarly to Ijjász-Vásquez et al. (1992). They found that the evolved landscapes have sharp hillslope-valley transitions at a critical value of topographic index. These transitions were smoothed by treating precipitation as a random process with an exponential distribution, rather than having a single value. However, the topographic index type models neglect the role of nonlinearities in groundwater flow, and antecedent conditions that determine catchment runoff response to precipitation. Flow nonlinearity affects the degree to which groundwater flow is driven by diffusion of the water table rather than advection due to slope gradients of permeability contrasts, and can have significant effects on runoff generation (C. Harman & Sivapalan, 2009). The steady state assumption of the topographic index model assumes that a storm event is effectively independent of prior events, and arrives with the full subsurface capacity available to drain flow. Many hydrological studies have shown that antecedent conditions are important controls on runoff magnitudes, where wetter systems are primed for larger runoff response due to lack of available subsurface storage or transport capacity (Brocca et al., 2009; Tramblay et al., 2010).

Several studies have coupled landscape evolution with hydrological processes in greater detail. Huang and Niemann (2006, 2008) developed a coupled groundwater model and LEM, and demonstrated the importance of dynamic runoff generation mechanisms for the topographic evolution of different areas of modeled basins. Huang and Niemann (2006) focused on the evolution of a single well-studied catchment, and found that as they simulated its evolution from present, runoff was increasingly generated by subsurface lateral flow rather than saturation excess overland flow. Huang and Niemann (2008) explored the long-term geomorphic evolution of synthetic catchments with groundwater flow, and concluded that the hypsometry of steady state landscapes was not generally distinguishable between surface-water-dominated and groundwater-dominated landscapes.

In this case, sensitivity of modeled topography to parameters was conducted by imposing changes on the slope-area relationship rather than examining results of the coupled model, making it more difficult to evaluate the precise role of groundwater flow in long term evolution. Zhang et al. (2016) presented a highly detailed, coupled hydrological model and LEM, though to our knowledge it has not been used beyond the initial proof of concept. With solutions to Richards equation for subsurface flow and St. Venant's equation for surface flow and employment of several dozen parameters, this model is computationally expensive and may be more complex than needed to explore process feedbacks between shallow subsurface hydrology and landscape evolution. A systematic approach is needed to understand these feedbacks. It must be simple enough for interpretation of process controls while still having the core elements of landscape evolution and dynamic runoff generation from the shallow subsurface.

1.3 Approach

In this study, we develop and use a new groundwater-landscape evolution model to explore how subsurface-mediated runoff generation affects long-term catchment evolution. The model solves hydraulic groundwater equations to predict the water table location given prescribed recharge. Water in excess of the subsurface flow capacity becomes overland flow, which may detach and transport sediment, altering topographic properties that in turn affect runoff generation. Our model can support recharge rates which vary in space and time, but here we constrain the scope to considering only steady, uniform recharge. In order to generalize our understanding from the model results, we conduct a similarity analysis that provides new insight into the dynamics behind the widely used "stream power plus diffusion" model by reconciling contradictory dimensional analyses provided by Theodoratos et al. (2018) and Bonetti et al. (2020). We can reduce the seven dimensioned parameters of the model to four dimensionless parameters, one of which is always negligible. We present numerical results confirming the efficacy of our nondimensionalization and exploring the newly defined non-dimensional parameter space to determine how hydrologic and geomorphic parameters determine emergent hydro-geomorphic properties at geomorphic steady state. The results show that subsurface flow capacity relative to recharge rate exerts a fundamental control on hillslope length and relief, and that three topographic metrics derived from the governing equations form a natural basis for evaluating the resulting coevolved landscapes. We derive and discuss a theoretical relationship between these metrics that allows us to recover the key model input parameters (including subsurface transmissivity) from topographic analysis of the landscape. We conclude by discussing the possibilities this analysis may open for topographic analysis of humid upland landscapes that could inform quantitative understanding of hydrological processes at the landscape scale.

2 Governing equations

To investigate the effects of subsurface hydrology on landscape evolution, we couple a hydrological model to a standard model of landscape evolution. First, we derive a governing equation for topographic evolution that includes the role of space- and time-variable runoff in fluvial incision. Second, we examine the hydrological model that will generate runoff. Variable dimensions are provided in Sec. 9.

2.1 Landscape evolution

Topographic elevation $z(x, y, t)$ is assumed to evolve due to fluvial incision $E_f(x, y, t)$, hillslope diffusion $E_h(x, y, t)$, and constant baselevel change U.

$$\frac{\partial z}{\partial t} = -E_f - E_h + U \tag{1}$$

The term E_f accounts for incision into the landscape by erosion due to overland flow. The term E_h accounts for gravitational soil-transport processes that tend to smooth out landscape features. The term U accounts for the constant rate of either tectonic uplift or baselevel fall, in this case increasing topographic elevation relative to a fixed elevation boundary.

In one commonly used form of this equation, fluvial incision is described by the streampower law, originally derived from empirical data (Howard & Kerby, 1983):

$$E_f = KA^m|\nabla z|^n \tag{2}$$

Here $A(x, y, t)$ is the upslope drainage area. In the standard streampower formulation, the exponents are $m = 1/2$ and $n = 1$. This is supported by observations of stream profile concavity that suggest $m/n \approx 0.5$, and a derivation in which incision is proportional to streampower per unit surface area, and channel width increases with the square root of discharge (Whipple & Tucker, 1999; Barnhart, Tucker, Doty, Shobe, et al., 2020). This gives the streampower incision law:

$$E_f = K\sqrt{A}|\nabla z| \tag{3}$$

This equation obscures the role of hydrological processes in the fluvial incision that drives landscape evolution. The relationship in (3) can also be derived from first principles in a way that provides a natural coupling to hydrological processes. This is accomplished by assuming the incision rate E_f is related to the excess shear stress τ from overland flow by some relationship. Frequently, this is written in the form:

$$E_f = k_e(\tau - \tau_c)^\beta \tag{4}$$

This excess shear stress formulation assumes that sediment is not redeposited within the domain (meaning that the system is assumed to be "detachment-limited"), which is widely used for upland watersheds (Howard, 1994). The shear stress generated by steady, uniform flow in a rectangular channel is:

$$\tau = \rho_w g d_f |\nabla z|, \tag{5}$$

where ρ_w is the density of water, g is the acceleration due to gravity, and d_f is the flow depth. A constitutive relation for flow resistance such as the Manning or Chezy equation can provide the flow depth d_f at a particular discharge Q. We use the Chezy equation for simplicity, which gives:

$$d_f = \left(\frac{Q}{Cw\sqrt{|\nabla z|}}\right)^{2/3} \tag{6}$$

Here we assume that the channel width w is proportional to the square root of upslope area (e.g., Snyder et al., 2003; Wohl & David, 2008):

$$w \sim \sqrt{A} \tag{7}$$

As we will show in subsequent scaling analysis, it will be useful to express this relation in terms of area per contour width $a(x, y, t)$. However, the hydraulic scaling relationships for channel width are defined on the basis of catchment area A at a given cross section (Leopold & Maddock, 1953). To make the conversion between A and a, we represent A as the product of a and a characteristic contour width v_0, which is a chosen constant value. We will examine the physical significance of this parameter in later sections.

To obtain values for w from the expression (7) we additionally require the dimensionless parameter k_w:

$$w = k_w \sqrt{v_0 a} \tag{8}$$

In this equation there is only one degree of freedom, so we are free to choose a value of v_0 for which there will always be a corresponding value of k_w to satisfy a given relationship between a and w. Ultimately, k_w will become a component of the streampower coefficient K, while here v_0 remains separate, and has additional significance in the context of hydrological processes.

Next, we write the discharge $Q(x, y, t)$ as the product of an instantaneous runoff ratio $Q^*(x, y, t)$, upslope area A, and the average recharge rate p, $Q = pAQ^*$, and substitute into (5) and (6) to find the flow depth and shear stress.

$$d_f = \left(\frac{Q^* p \sqrt{v_0 a}}{C k_w \sqrt{|\nabla z|}} \right)^{2/3} \tag{9}$$

$$\tau = \rho_w g \left(\frac{Q^* p \sqrt{v_0 a}}{C k_w \sqrt{|\nabla z|}} \right)^{2/3} |\nabla z| \tag{10}$$

To recover the the stream power formulation of the fluvial incision term, we set $\beta = 3/2$ (Tucker, 2004) in (4), representative of hydraulic detachment by plucking (Whipple et al., 2000; Tsujimoto, 1999). With these substitutions, the incision rate E_f can be written as:

$$E_f = K \sqrt{v_0} Q^* \sqrt{a} |\nabla z| \tag{11}$$

where $K = \frac{(\rho_w g)^{3/2} k_e p}{C k_w}$. This form is equivalent to (3), with time and space varying runoff accounted for in Q^*. Additionally because Q^* is dimensionless, K in (11) has units of $[1/T]$, the same as in (3).

The upslope area A is usually defined by explaining the algorithms used to calculate it in numerical schemes, which find flow directions on a discrete grid and sum the grid cell areas downslope along these flow directions. However, this approach gives the area an implicit dependence on grid cell spacing. Area per contour width a on the other hand has a precise mathematical definition that can be derived from conservation of mass (Bonetti et al., 2018, 2020). Consider the steady state depth of water h_f across a surface where all locations contribute runoff at the same rate r. Conservation of mass for this system indicates that $\nabla \cdot (h_f u) = r$, where u is the (vector) flow velocity. Now suppose that the flow velocity at every point also has magnitude r and points in the direction of steepest descent $-\nabla z / |\nabla z|$. To satisfy continuity with this velocity, the flow depth must be equal to the upslope area per contour width, $h_f = a$ (Bonetti et al., 2018). This derivation shows that, by definition:

$$-\nabla \cdot \left(a \frac{\nabla z}{|\nabla z|} \right) = 1 \tag{12}$$

We are not implying that the assumptions we have made here are necessarily characteristics of all real flow; rather these assumptions can be employed, without violating conservation of mass, to derive an expression for area per contour width as a function of the local terrain. This expression will become important in our scaling analysis in later sections, as the scaling properties of the governing equations should be independent of the numerical implementation where a grid cell width must be chosen.

Here we use a linear diffusion model of hillslope processes for E_h, which emerges by assuming that the non-fluvial sediment transport rate q_h is proportional to the local slope gradient $-\nabla z$, much as diffusion of a solute is proportional to the concentration gradient (Dietrich et al., 2003). Then by assuming $E_h \sim -\nabla \cdot q_h$ from continuity, we find:

$$E_h = D\nabla^2 z, \tag{13}$$

where D is the linear diffusion constant. While nonlinear formulations of diffusion have proven useful in explaining topography (Roering et al., 1999; Roering, 2008), here we use linear diffusion to limit model complexity. We assume that baselevel change has a constant rate U in time and space by adopting a frame of reference anchored to baselevel at the boundary of the domain. This can equivalently represent tectonic uplift or baselevel fall. This term becomes a "source" in the differential equation; without it, the topography would simply erode to a flat plane. While baselevel change is likely not steady in time in real landscapes, this assumption allows us to examine the emergent properties of steady-state solutions to the governing equation. Combining all terms together, we arrive at our governing equations for topographic evolution:

$$\frac{\partial z}{\partial t} = -K\sqrt{v_0}Q^*\sqrt{a}|\nabla z| + D\nabla^2 z + U \tag{14}$$

$$-\nabla \cdot \left(a\frac{\nabla z}{|\nabla z|} \right) = 1 \tag{15}$$

This is different from the standard streampower formulation of landscape evolution in that it includes a dimensionless runoff coefficient Q^* to account for the spatial and temporal variation in runoff across the landscape. While there is considerable uncertainty in the form of the fluvial incision term, the similarity between the form we have selected and the standard "stream power plus diffusion" formulation allows us to make use of the same nondimensionalization techniques used for the standard LEM, and has properties that will aid in implementation and analysis of results while remaining plausible within the context of the existing literature.

2.2 Hydrology

Thus far, we have made no assumptions regarding the hydrology, instead introducing $Q^* = Q/(pA)$. Any approach to representing hydrology could use the above equations by calculate appropriate values for Q^*. In our application surface water runoff is assumed to be generated by exfiltrating subsurface lateral flow (Hewlett & Hibbert, 1967) and by precipitation on saturated areas (Dunne & Black, 1970). We solve for this runoff using a quasi-3D shallow unconfined aquifer model using the Dupuit-Forcheimer approximations (e.g., Childs, 1971). This model makes use of a method of regularization introduced by Marçais et al. (2017) that greatly improves model stability at seepage faces. We solve the model for lateral groundwater flow $q(x, y, t)$, and local runoff production $q_s(x, y, t)$. Surface water discharge is calculated by instantaneously routing q_s and summing the accumulated local runoff over the area upslope of a given location. The governing equations for the hydrological model are:

$$\frac{\partial h}{\partial t} = \frac{1}{n}\left(p - \nabla \cdot q - q_s\right) \tag{16}$$

$$q = -h\cos\theta k_s\left(\nabla z + \nabla h\right)\cos\theta \tag{17}$$

$$q_s = \mathcal{G}\left(\frac{h}{b}\right)\mathcal{R}\left(i - \nabla \cdot q\right) \tag{18}$$

$$Q = \int_A q_s dA \tag{19}$$

where $h(x, y, t)$ is the aquifer thickness, n is the drainable porosity, $\theta(x, y, t)$ is the local slope of the (presumed impermeable) aquifer base, and b is the permeable thickness. The regularization function $\mathcal{G}(\cdot)$ has a value of zero when the argument is less than one, and approaches 1 as the argument approaches 1. The ramp function $\mathcal{R}(\cdot)$ is zero when the argument is less than zero and takes on the argument value when it is greater than zero.

Though this model can accommodate time-variable recharge, here we consider only constant recharge at rate p. Careful examination of this model reveals that saturated areas receive "recharge" at the same rate as areas with deeper water tables. In reality, saturated areas receive direct precipitation, while areas with deeper water tables receive a smaller fraction as a result of losses to unsaturated zone storage and evapotranspiration from the root zone. When saturated area is a small proportion of the total area and the water table is not too deep, this effect may be negligible. We will leave further investigation on the role of unsaturated zone dynamics to a future contribution, as this would add considerable complexity to the model.

In the cases modeled here, the permeable thickness b is treated as constant in space and time. Considerable uncertainty exists in the rates and mechanisms that convert fresh bedrock to permeable fractured rock and/or regolith. Many past models have used an exponential function for the production of regolith (e.g., Ahnert, 1976; Armstrong, 1976; Rosenbloom & Anderson, 1994; Tucker & Slingerland, 1997), where the production rate is a function of regolith thickness. At geomorphic steady state, both the rates of change of topographic elevation and unweathered bedrock elevation go to zero. For the latter to be the case, the regolith production rate must be equal to the uplift rate. When the uplift rate and regolith production coefficients are spatially uniform, regolith thickness must be also be uniform to satisfy this equilibrium. This suggests that it is reasonable to treat permeable thickness as steady and uniform across the model domain given that we are only concerned with steady state landforms in this paper.

3 Numerical implementation

3.1 Timescale considerations

One of the primary challenges in coupling a hydrological model with a landscape evolution model is the vast difference in process timescales. While the relevant timescale for storm runoff response may be on the order of hours or even minutes, landscape evolution processes can have characteristic timescales in the tens to thousands of years. It would be too computationally expensive to run models over geologic time using appropriately small timesteps for stability and accuracy of the hydrological model. Zhang et al. (2016) identified two approaches to address this problem: online updating and offline updating. In the offline case, the hydrological model is run for many steps without updating topography, and then appropriately averaged discharge values are used to update topography over some larger geomorphic timestep. In contrast, online updating involves having a direct scaling between the hydrological timestep (e.g., one storm event) and the geomorphic timestep. Zhang et al. (2016) use an online approach, citing possible non-

uniqueness of solutions in the offline approach depending on the time between geomorphic updates. Given that we consider only steady recharge in this paper, there should not be a significant difference between online and offline approaches given that the hydrological state varies gradually, only in response to changing topography. Nonetheless, our approach can be considered online updating, as we scale the geomorphic timestep as k_{sf} times the hydrological timestep: $\Delta t_g = k_{sf} \Delta t_h$.

3.2 Model implementation

The groundwater and landscape evolution models described above were implemented as the `DupuitLEM` Python package, which makes extensive use of existing tools from the Python-based Earth surface modeling toolkit Landlab (Hobley et al., 2017; Barnhart, Hutton, et al., 2020). Landlab includes tools for creating grids, setting boundary conditions, handling input and output, along with a diverse range of process components that modify fields on Landlab grids according to physical laws. The groundwater model described above is implemented as a component in Landlab called `GroundwaterDupuitPercolator` (Litwin et al., 2020).

`DupuitLEM` can handle raster, hexagonal, and irregular grids, along with zero-flux and fixed-value boundary conditions. The model base class takes components that update the hydrological state via hydrological fluxes and changes in boundary conditions, update topography via fluvial incision and hillslope diffusion, and update topography and regolith thickness via baselevel change and regolith production. Here we use the `DupuitLEM` subclass `StreampowerModel`, designed for use with the Landlab fluvial incision component `FastscapeEroder`, which solves a modified version of the Fastscape algorithm (Braun & Willett, 2013).

The hydrological state is updated with a `DupuitLEM` `HydrologicalModel`. All hydrological models solve for aquifer state and fluxes using the `GroundwaterDupuitPercolator` component. Surface water discharge is routed instantaneously using a D8 algorithm when the grid is a raster, or a steepest descent algorithm otherwise. In the case of steady recharge, we use the `HydrologicalModel` subclass `HydrologySteadyStreamPower`, which updates the surface water discharge by advancing the `GroundwaterDupuitPercolator`, finding surface flow directions including routing through topographic depressions, and accumulating q_s along flow directions to determine Q. With known area A and recharge rate p, we can calculate the runoff ratio $Q^* = Q/(pA)$ that appears in our streampower model, linking the hydrology to geomorphic evolution. We use a raster grid with dimensions 125x125, with three zero flux boundaries (right, left, top) and one fixed value boundary along the bottom of the model domain. The geomorphic timestep is kept constant at 45 years, while the hydrologic timestep varies as a multiple of the von Neumann stability criteria, taking values from approximately four hours to three days. The adaptive timestep solver of the `GroundwaterDupuitPercolator` will further subdivide the timestep to meet stability criteria, while surface flow is only routed at this interval.

4 Scaling and similarity

A similarity analysis of the governing equations illuminates their fundamental controls and will guide the investigation conducted in the rest of this paper. Here we use an approach based on the concept of symmetry groups (Barenblatt, 1996). In essence, we seek to identify the complete set of scaling transformations of the governing equations under which the solutions are invariant, and then apply transformations to consolidate or eliminate parameters. This is an alternative approach to arrive at a general form of the governing equations where parameters emerge in dimensionless groups that can be varied in numerical experiments. We will begin this process by considering the simplest version of the model without space or time variable hydrology, where $Q^*(x, y) = 1$ everywhere. We will call this the *NoHyd* model. Theodoratos et al. (2018) determined

that there are unique characteristic scales for the vertical coordinate, the horizontal coordinate, and time h_g, ℓ_g, t_g that emerge from the streampower-linear diffusion landscape evolution equations. The comparable scales for our governing equation are slightly different, as we use the area per contour width a as a state variable rather than using area A. Based on the analysis of Theodoratos et al. (2018), we can rewrite equations (14) and (15) in terms of these scales without changing the units of the state variables.

$$t_g \frac{\partial z}{\partial t} = -\sqrt{\ell_g} Q^* \sqrt{a} |\nabla z| + \ell_g^2 \nabla^2 z + h_g \tag{20}$$

$$-\nabla \cdot \left(a \frac{\nabla z}{|\nabla z|} \right) = 1 \tag{21}$$

Because we have replaced three parameters, K, D, and U, with three characteristic scales h_g, ℓ_g, and t_g, without changing the state variables, we can solve for the three characteristic scales in terms of the model parameters:

$$h_g = \left(\frac{DU^3}{v_0^2 K^4} \right)^{1/3} \tag{22}$$

$$\ell_g = \left(\frac{D^2}{v_0 K^2} \right)^{1/3} \tag{23}$$

$$t_g = \left(\frac{D}{v_0^2 K^4} \right)^{1/3} \tag{24}$$

A physical law should remain valid regardless of the units that quantities are expressed in. This endows physical laws with certain symmetries under scaling of the dimensioned variables. There are three ways to scale two or more dimensioned variables by an arbitrary factor $c > 0$ that leave equations (20) and (21) unchanged.

$$\{t \to ct, t_g \to ct_g\} \tag{25}$$

$$\{z \to cz, h_g \to ch_g\} \tag{26}$$

$$\{x \to cx, y \to cy, a \to ca, l_g \to cl_g\} \tag{27}$$

Note that the final transformation also requires that $\nabla^2 z \to c^{-2} \nabla^2 z$ and $|\nabla z| \to c^{-1} |\nabla z|$, which are a consequence of the first two elements of the transformation.

These transformations can be applied as many times as desired, in any order, for any $c > 0$, and the equations remain the same because the factors c will always cancel. For this reason, we can also choose values of c such that the characteristic scales do not appear in the equations. For example, we can apply the first transformation, taking $c = 1/t_g$, we have the transformation $\{t \to t/t_g, t_g \to 1\}$. By doing this, we have effectively rescaled t into units relative to t_g. We will call this new time $t' = t/t_g$. Likewise, we can do this with the other transformations:

$$\begin{aligned} &\{t \to t/t_g, t_g \to 1\} \\ &\{z \to z/h_g, h_g \to 1\} \\ &\{x \to x/\ell_g, y \to y/\ell_g, a \to a/\ell_g, l_g \to 1\} \end{aligned} \tag{28}$$

We apply all three transformations to define dimensionless state variables:

$$\begin{aligned} t' &= t/t_g \\ z' &= z/h_g \\ x' &= x/\ell_g \\ y' &= y/\ell_g \\ \nabla' &= \nabla \ell_g \\ a' &= a/\ell_g \end{aligned} \tag{29}$$

and express the governing equations for the landscape evolution model:

$$\frac{\partial z'}{\partial t'} = -\sqrt{a'}|\nabla' z'| + \nabla'^2 z' + 1 \tag{30}$$

$$-\nabla' \cdot \left(a' \frac{\nabla' z'}{|\nabla' z'|} \right) = 1 \tag{31}$$

No parameters appear in these rescaled equations. This would not be the case if we had chosen to write the equations in terms of area A and not area per unit contour width a, as a single parameter of v_0/ℓ_g would appear in equation (31). Not accounting for this parameter effectively leaves a grid cell size dependence in the nondimensionalization, which is something we seek to avoid.

Next we relax our constraint of $Q^* = 1$ and incorporate the hydrology equations into the scaling analysis. This model is called *DupuitLEM*. Because the hydrological model is linked to the geomorphic model through the dimensionless variable Q^*, the set of transformations used for the geomorphic equations above is not necessarily applicable to the *DupuitLEM* model. In addition to the characteristic scales used for the *NoHyd* model, ℓ_g, h_g, and t_g, we will introduce three scales particularly relevant to the hydrological processes: a characteristic aquifer thickness h_c, a characteristic aquifer drainage time t_d, and the recharge rate p. A simple mass balance of water in a 1D hillslope with length ℓ_g, relief h_g, recharge rate p, and hydraulic conductivity k_s gives:

$$p\ell_g = h_c k_s h_g / \ell_g, \tag{32}$$

while the characteristic drainage time can be derived for a shallow aquifer can be derived from C. Harman and Sivapalan (2009, their eq. 6), which likewise describes the drainage of an aquifer with characteristic length and relief with drainable porosity n:

$$t_d = \frac{\ell_g n}{k_s \sin\theta} \tag{33}$$

Making the approximation $\sin(\theta) \sim h_g/\ell_g$, the resulting characteristic scales are:

$$h_c = \frac{p\ell_g}{k_s h_g/\ell_g} \tag{34}$$

$$t_d = \frac{\ell_g n}{k_s h_g/\ell_g} \tag{35}$$

$$p \tag{36}$$

In addition to the recast landscape evolution equations in (20) and (21), we add those of the hydrological model:

$$\frac{\partial h}{\partial t} = \frac{h_c}{t_d}\left(1 - \frac{\nabla \cdot q}{p} - \frac{q_s}{p}\right) \tag{37}$$

$$\frac{q}{p} = -h\cos^2(\arctan|\nabla z|)\frac{\ell_g^2}{h_g h_c}\left(\nabla h + \nabla z\right) \tag{38}$$

$$\frac{q_s}{p} = \mathcal{G}\left(\frac{h}{b}\right)\mathcal{R}\left(1 - \frac{\nabla \cdot q}{p}\right) \tag{39}$$

$$Q^* = \frac{1}{Ap}\int_A q_s dA_c \tag{40}$$

Here we have expanded the aquifer base angle θ as $\arctan|\nabla z|$, as constant permeable thickness implies that the aquifer base gradient is equal to the topographic gradient. As with the scaling analysis in equations (20) and (21), we can look for transformations under which the equations are invariant. While the scaling in the time dimension shown in (28) will apply as before, unlike in the geomorphic governing equations we cannot separately transform the vertical and horizontal length scales in the hydrologic equations. The aquifer specific discharge q cannot be separated from the topographic gradient ∇z due to the cosine term in (38). As a result, there are only two transformations that produce invariance:

$$\begin{aligned}&\{t \to ct, t_g \to ct_g, t_d \to ct_d\}\\ &\{x \to cx, y \to cy, a \to ca, A \to c^2 A, l_g \to cl_g,\\ &\quad q \to cq, z \to cz, h \to ch, h_g \to ch_g, h_c \to ch_c, b \to cb\}\end{aligned} \tag{41}$$

Again, we can choose scales c and apply the transformations in search of a form that eliminates or consolidates the characteristic scales. We will first apply the time transformation, choosing $c = 1/(t_g t_d)$. This is equivalent to applying the transformation twice, once with $c = 1/t_g$ and again with $c = 1/t_d$. We will then apply the second transformation, choosing $c = 1/(\ell_g h_g h_c)$. Likewise, this is equivalent to applying the transformation three times with each of the three factors in the denominator. In addition to the rescaled variables presented in (29), we add several additional rescaled variables:

$$\begin{aligned}h &= h' h_c\\ t &= t' t_d\\ q &= q' p \ell_g\\ q_s &= q_s' p\end{aligned} \tag{42}$$

Applying the two transformations, and employing the above definitions, we find find the governing equations simplify to the following:

$$\frac{\partial z'}{\partial t'} = - Q^* \sqrt{a'} |\nabla' z'| + \nabla'^2 z' + 1 \tag{43}$$

$$- \nabla' \cdot \left(a' \frac{\nabla' z'}{|\nabla' z'|} \right) = 1 \tag{44}$$

$$\frac{\partial h'}{\partial t} \frac{t_d}{t_g} = 1 - \nabla' \cdot q' - q'_s \tag{45}$$

$$q' = - h' \cos^2(\arctan |\nabla' z' h_g / \ell_g|) \left(\nabla' h' \frac{h_c}{h_g} + \nabla' z' \right) \tag{46}$$

$$= - h' \frac{\nabla' h' h_c / h_g + \nabla' z'}{1 + (h_g/\ell_g)^2 |\nabla' z'|^2} \tag{47}$$

$$q'_s = \mathcal{G}\left(h' \frac{h_c}{b} \right) \mathcal{R}\left(1 - \nabla' \cdot q' \right) \tag{48}$$

$$Q^* = \frac{1}{A'} \int_{A'} q'_s dA' \tag{49}$$

Our use of Q^* as a dimensionless representation of hydrology in the geomorphic equation means that we are still able to obtain a parameterless expression for topographic evolution, even though we have not separated the transformation of vertical and horizontal length scales in the hydrologic governing equations. There are, however, four parameter groups that we cannot eliminate. We will give them the following names, which will be used throughout the rest of this paper:

$$\delta = \frac{t_d}{t_g} = \frac{n\, v_0^{2/3} D^{2/3} K^{4/3}}{k_s U} \tag{50}$$

$$\alpha = \frac{h_g}{\ell_g} = \frac{U}{v_0^{1/3} D^{1/3} K^{2/3}} \tag{51}$$

$$\gamma = \frac{b}{h_c} = \frac{b k_s h_g}{p \ell_g^2} = \frac{b k_s U}{p D} \tag{52}$$

$$\mathrm{Hi} = \frac{h_g}{h_c} = \frac{k_s h_g^2}{p \ell_g^2} = \frac{k_s U^2}{p\, v_0^{2/3} D^{2/3} K^{4/3}} \tag{53}$$

Here δ represents the scaling between the hydrologic and geomorphic timescales of the model. By the nature of hydrologic and geomorphic processes, we expect this ratio to be very small in all cases. Additionally, δ multiplies the time rate of change of aquifer thickness, which should also be very small here as we only consider steady recharge. α is a characteristic gradient of the model that emerges from the geomorphic parameters. We will call γ the drainage capacity, as it is proportional to the maximum transmissivity and the characteristic topographic gradient and inversely proportional to the mean recharge rate. Hi is analagous to the Hillslope number Hi presented by Brutsaert (2005) (Eq. 10.139) and used by C. Harman and Sivapalan (2009), C. J. Harman and Kim (2019), and others to understand shallow groundwater dynamics. It represents the relative importance of topographic gradients, versus diffusion of the water table, in driving groundwater flow. It can be thought of as a Peclet number, as it captures the ratio of advective to diffusive processes.

4.1 Special cases

These equations and parameters all apply in the general case when aquifer and topographic gradients are important drivers of groundwater flow. The expressions can be simplified under conditions where one gradient is more important than the other, reducing the constraints on our symmetry groups. Suppose that relief is generally large in comparison to aquifer thickness, $h_g \gg h_c$, in which case $\mathrm{Hi} \gg 1$. Consequently, topographic gradients rather than aquifer thickness gradients tend to drive groundwater flow. In this case we neglect ∇h, altering the groundwater specific discharge expression (38):

$$\frac{q}{p} = -h\cos^2(\arctan|\nabla z|)\frac{\ell_g^2}{h_g h_c}\nabla z \tag{54}$$

Applying our symmetry method as before, we find that ℓ_g and h_g must still be scaled together. However, this time, h need not be scaled with these simultaneously in order to obtain a consistent set of equations. Instead, there are now three transformations that comprise the symmetry:

$$\begin{aligned}
&\{t \to ct, t_g \to ct_g, t_d \to ct_d\}\\
&\{h \to ch, h_c \to ch_c, b \to cb\}\\
&\{x \to cx, y \to cy, a \to ca, A \to c^2 A, l_g \to cl_g,\\
&\quad q \to cq, z \to cz, h_g \to ch_g\}
\end{aligned} \tag{55}$$

Implementing the three transformations above with $c = 1/t_g$, $c = 1/h_c$, and $c = 1/(h_g\ell_g)$ respectively, we arrive at a rescaled set of governing equations similar to previous, only with an altered expression for q':

$$q' = -h'\cos^2(\arctan|\nabla' z' h_g/\ell_g|)\nabla' z' \tag{56}$$

Here the factor $\mathrm{Hi} = h_g/h_c$ no longer appears in the equation. This suggests that the solution to the full governing equations should be independent of Hi when Hi is large. This makes sense in the context of Equation (47), as $1/\mathrm{Hi}$ multiplies the gradient in aquifer thickness, which by definition will be small relative to topographic gradients when Hi is large.

Conversely, suppose that topographic gradients were largely insignificant, and flow was generally driven by gradients in aquifer thickness ($\nabla h \gg \nabla z$). In this case, the expression for groundwater specific discharge changes again, as we can approximate $\cos\theta \approx 1$ and $\nabla z \approx 0$ for the purposes of groundwater flow. Then the governing equations are again the same except for q:

$$\frac{q}{p} = -h\frac{\ell_g^2}{h_g h_c}\nabla h \tag{57}$$

In this case, because the cosine term does not appear, ℓ_g and h_g need not be scaled together. As in the previous case, there are three transformations that maintain symmetry, with a separate scaling for aquifer thickness h. However, in order to maintain consistency in the groundwater specific discharge equation, the vertical coordinate and h_g must be scaled with h.

$$\begin{aligned}
&\{t \to ct, t_g \to ct_g, t_d \to ct_d\} \\
&\{h \to ch, h_c \to ch_c, b \to cb, z \to cz, h_g \to ch_g\} \\
&\{x \to cx, y \to cy, a \to ca, A \to c^2 A, l_g \to cl_g, q \to cq\}
\end{aligned} \tag{58}$$

Noting that these transformations are simply a rearrangement of the previous, we select the scales $c = 1/t_g$, $c = 1/(h_c h_g)$, and $c = 1/\ell_g$ respectively. We arrive at a rescaled set of governing equations when flow is primarily driven by gradients in aquifer thickness. Only the expression for q' has changed:

$$q' = -h' \frac{\nabla' h'}{\mathrm{Hi}} \tag{59}$$

Under these conditions, the factor $\mathrm{Hi} = h_g/h_c$ still appears in the groundwater specific discharge expression, while the parameter $\alpha = h_g/\ell_g$ no longer appears. This suggests that as Hi becomes small, the sensitivity to Hi does not decrease, but sensitivity to α does decrease. Small Hi indicates that water table gradients are more important than topographic gradients in driving flow. As α is a measure of topographic gradients, it is appropriate that it should diminish in importance when Hi is small. The two end-member scenarios, where hydraulic gradients are alternately driven by topography or aquifer thickness, provide insight into expected parameter sensitivity, which we will test with the numerical model. In particular, we expect that for low values of Hi, the solution should be generally insensitive to the value of α, while the sensitivity to Hi will be small for high values of Hi. Overall, we have reduced the governing equations from a system with 7 parameters to a system with 4 parameters, one of which we expect one to be unimportant in all cases (δ). This significantly improved our ability to explore and comprehend the parameter space in the following sections.

5 Results

We explore the properties of the scaled model through a series of simulations designed to sample the nondimensional parameter space of α, γ, and Hi. While the fourth dimensionless parameter, δ, does vary as we vary hydrological parameters, this effect should be negligible for reasons previously stated.

We consider two cases of simulations. First, simulations with the *NoHyd* model in which $Q^* = 1$ and second, simulations with *DupuitLEM* in which Q^* varies in space and time. Such variation may arise under steady, uniform recharge as shallow subsurface aquifer does not uniformly exfiltrate. Here time variation of Q^* is only due to changes in geomorphic boundary conditions. Additional complexity could be added by considering time and/or spatially varying recharge—we do not consider this here. We evaluated the condition of steady state topography on the basis of change in mean dimensionless relief R_h/h_g, where R_h is the mean value of elevation z. For runs of the *NoHyd* model and runs of the *DupuitLEM* model where $\gamma < 1$, the results show clear indications of steady state, as the absolute value of dimensionless rate of relief change $|\frac{dR_h/hg}{dt/t_g}|$ declines below 10^{-10}. In cases with larger γ, perturbations continue through time in the absolute value of relief change. We run the model at least until there is no decreasing trend in the absolute value of relief change. Times to meet these conditions range from approximately 300-2000 t_g, around 7-45 million years.

5.1 Confirmation of scaling and similarity

The numerical results confirm the scaling predicted in our similarity analysis. In Figure 1A (i, ii, iii) we show that ℓ_g can be varied independently from h_g (changing α)

with the *NoHyd* model and we can still obtain visually and numerically identical results in the rescaled coordinate system (x', y', z'). The same similarity appears when h_g is varied independently while ℓ_g remains constant (i, iv, vi) and when h_g and ℓ_g are varied together (i, v, vii). The mean absolute difference in z' between all model runs is less than 10^{-13}% of total relief. These results confirm the scaling found by Theodoratos et al. (2018), showing that the vertical and horizontal dimensions possess distinct and independent scaling relationships. Our similarity approach also predicts that the vertical and horizontal length scales should not scale independently in the *DupuitLEM* model, unless Hi $\ll$ 1. Figure 1B shows the same scaling of h_g and ℓ_g implemented in Figure 1A, now using the *DupuitLEM* model with Hi $= 5$ and $\gamma = 2.5$. As ℓ_g is increased independent of h_g (i, ii, iii), α decreases and the distance between channels appears to increase. Similarly as we increase h_g while holding ℓ_g constant (i, iv, vi), α increases and we observe a decrease in spacing between channels. It is only when h_g and ℓ_g are varied together (i, v, vii), keeping α constant, that topography remains invariant in the rescaled coordinates. There is less than 2% difference in mean relief between the results in (i, v, vii). While sufficient to confirm the scaling analysis, this difference is larger to that observed in 1A due to isolated areas that develop slightly different drainage patterns. This is likely as a result of small numerical differences between the groundwater model solutions early in the evolution of topography.

Our similarity analysis suggested that vertical and horizontal dimensions should scale independently when Hi is small. In this case, relief is small relative to the characteristic aquifer thickness, and as a result it should not play a strong role in generating hydraulic gradients that drive flow. Figure 1C shows the results of the same variation in h_g and ℓ_g as Figure 1B, but now with Hi $= 0.01$. In this case, h_g and ℓ_g appear to scale independently for relatively small values of α (< 0.2). Plots (i, iv, vi) do still show some topographic variation between model runs, while (i, ii, iii) do not. While this provides some confirmation of our scaling analysis, in the cases we will test going forward, Hi values will generally not be small enough for the results to be independent of α.

5.2 Sensitivity to dimensionless hydrologic parameters

The results suggest that landscape and climate properties affecting shallow groundwater flow could have major effects on topography. There are strong differences in topography between model runs when dimensionless parameters describing these factors are varied. In particular, the evolved topography is strongly dependent on the drainage capacity γ, which is the ratio of soil depth b to characteristic aquifer thickness $h_c = \frac{p\ell_g^2}{k_s h_g}$. When $\gamma = 0.5$, the lowest value shown in Figure 2, the results look very similar to those obtained with the *NoHyd* model. In these cases the entire landscape experiences some overland flow and erosion, which is apparent in the spatial distribution of Q^* shown in Figure 4. In contrast, high γ cases produce broad interfluves where $Q^* = 0$, as the water table sits further below the surface. As a result these areas do not experience surface erosion. To a lesser degree, Hi affects the steady state topography as well. As discussed previously, Hi describes the characteristic relief relative to the characteristic aquifer thickness. From the the hillshades presented in Figure 2, it appears that Hi has the greatest influence on topography when drainage capacity γ is large, in which case increasing Hi generally decreases the spacing between channels. The previous section evaluating the scaling properties of the model results showed that α has a significant effect on topography in most cases where Hi is not very small. The supplemental material includes figures showing the results of varying γ and Hi with higher and lower values of α than those shown here. While transitions in morphology and runoff happen at different values of γ and Hi when α is varied, the fundamental dependence on these parameters remains the same.

Distributions of Q^* represent the spatial variability in runoff that emerges from our coupled geomorphic-hydrologic model under conditions of steady, uniform recharge. These

distributions confirm that the extent of areas contributing runoff tends to decrease with increasing γ, and to a lesser extent with decreasing Hi. Figure 4B shows cumulative distribution functions of Q^* for each model run, indicating the proportion of the landscape where Q^* is less than a particular value on the x-axis. Strikingly, we see that areas that contribute no runoff ($Q^* = 0$) first appear exactly when $\gamma = 1$ (third row from the bottom). This holds for smaller and larger values of α as well (see Figures S3, S6). It is at this point that the spatial variability in Q^* is maximized: at lower values all areas contribute some runoff, while above this value, most areas contribute no runoff at all. As γ is the ratio of the characteristic aquifer thickness h_c to the permeable thickness b, a value of 1 should indicate that a "characteristic hillslope" has just become saturated, which appears to be in agreement with our results. This is a powerful demonstration of the effectiveness of this nondimensionalization.

In Figure 4C, the proportion of computational grid nodes with $Q^* > 0.5$ indicates extensive saturation in low γ cases with minor sensitivity Hi values; the extent of runoff contributing areas declines slightly more rapidly when Hi is large. For comparison, we also plot the proportion of the landscape with positive curvature, which shows a more gradual change with γ.

Clearly subsurface hydrology is having a strong effect on topography in this model. With increasing ability to drain water through the subsurface (large γ), less surface drainage is needed, and consequently, the spacing between streams is greater. Furthermore, landscapes with lower drainage capacity (smaller γ) have larger source areas of overland flow extending across more the landscape. When drainage capacity is larger, the landscape is generally steeper and saturated areas are restricted to narrow incised regions. The patterns of Q^* indicate that $\gamma = 1$ defines the transition between landscapes that evolve with these two behaviors.

6 Emergent properties at landscape equilibrium

6.1 Topographic analysis: steepness and curvature

The landscapes shown in Figures 1, 2 and 4 reveal the visually striking influence of hydrological properties on landscape form. However, there is still much more we can learn about the controls on these emergent properties, guided by the form of the governing equations. Furthermore, we would like to be able to develop some quantitative understanding that relates readily observable topographic features to hydrological properties that are more difficult to measure. The relationships between model parameters and emergent hydrologic and geomorphic properties will be the focus of this section.

Commonly, properties of stream channels and entire landscapes are examined by plotting local slope versus accumulated area (e.g., Tarboton et al., 1989; Willgoose, Bras, & Rodriguez-Iturbe, 1991; Dietrich et al., 1993). Results form point clouds where zones of distinct behavior can be identified (Perron et al., 2008). Recently, Theodoratos et al. (2018) showed that the topography resulting from the streampower-linear diffusion LEM may be analyzed by examining relationships between what they term the incision height $\sqrt{A}|\nabla z|$ and Laplacian curvature $\nabla^2 z$. (Theodoratos & Kirchner, 2020b) refer to $\sqrt{A}|\nabla z|$ as steepness, so here we will adopt similar terminology, with one difference: to match the form of our governing equations, we define steepness as $\sqrt{a}|\nabla z|$, using area per contour width a rather than area A. Steepness and curvature emerge naturally from the steady state form of the governing equation for topographic evolution (20). Setting the time rate of change equal to zero, and rearranging, we obtain the following relationship:

$$\nabla^2 z = \ell_g^{-3/2} Q^* \sqrt{a}|\nabla z| - \frac{h_g}{\ell_g^2} \tag{60}$$

which has the equivalent dimensionless form:

$$\nabla'^2 z' = Q^* \sqrt{a'} |\nabla' z'| - 1 \tag{61}$$

When runoff generation is spatially uniform and therefore $Q^* = 1$ for all (x, y), as in the *NoHyd* model, there is a linear relationship between steepness and curvature, with a slope of unity and intercept of -1 in dimensionless coordinates, as observed by Theodoratos et al. (2018). While this definition of steepness is contingent on the particular exponents on area and slope, Theodoratos et al. (2018) showed that this relationship can be generalized to any exponent values, albeit with significantly more complicated formulas.

Figure 5 shows topography from a run of the *NoHyd* model in slope-area and steepness-curvature space. The results show the expected slope and intercept in the steepness-curvature plot. All of the variability that appears in the slope-area space collapses onto a single line in steepness-curvature space, making steepness-curvature plots powerful tools for examining model behavior. Observing this relationship in the numerical solution also demonstrates that the model accurately reproduces the analytical result at steady state.

Furthermore, deviations created by the introduction of hydrologic variability with Q^* should be readily apparent when plotting steepness versus curvature. When we use the *DupuitLEM* model, plotting $Q^* \sqrt{a'} |\nabla' z'|$ rather than $\sqrt{a'} |\nabla' z'|$ versus curvature would again result in a linear relationship. Through topographic analysis alone, however, steepness and curvature are available while Q^* is not. Quantifying the relationship between these topographically-derived quantities and Q^* across each steady state landscape in our nondimensional parameter space thus supports quantifying hydrological function based upon topography.

Slope-area and steepness-curvature plots for selected model runs with different values of γ and Hi are shown in Figure 6. The steepness-curvature relationships for the low γ cases show close agreement with the theoretical relationships derived from the *NoHyd* model (dotted black line). This is consistent with the observed values of Q^*, which are close to unity at most nodes. With increasing drainage capacity γ, there is an apparent separation between points that conform to the theoretical relationship and points that maintain constant negative curvature $\nabla^2 z = -h_g / \ell_g^2$. The difference between these behaviors is revealed in the values of Q^*. Areas in yellow have $Q^* \approx 0$, and form the zone of constant negative curvature. This is exactly what we would expect from the solution to the steady state equation (61) in the absence of the fluvial incision term. Points in this zone are divergent hillslopes that do not reach surface saturation. Areas in blue have $Q^* \approx 1$, essentially conforming to the same relationship observed for the *NoHyd* model. Points in this zone are the fluvial valleys that are fully saturated and have discharge approximately equal to upslope area times the recharge rate. This indicates that at these locations the vast majority of water is moving over the surface rather than through the subsurface. A limited number of points fall in between these two end members of behavior. These are the channel heads and other areas of limited runoff contribution, where $0 < Q^* < 1$. When $\gamma > 1$, the proportion of points in this intermediate space appears to decrease with increasing γ.

Slope-area plots do show separation between these behaviors, though the end members of behavior are not nearly as distinct. Differences between channel and hillslope morphology are also apparent in map view plots of steepness and curvature (Figure 7). While steepness does seem to provide an indication of increasing channelization in the low γ cases, in the high γ cases, it takes on unusual swirling patterns on hillslopes, in part due to the D8 flow routing method. These are of little consequence in the context of processes acting in the model, because on these hillslopes $Q^* \to 0$ and therefore the fluvial incision term that also goes to zero. Map view curvature plots show that in low γ cases, areas of negative curvature are restricted to narrow areas near the ridges, while exten-

sive areas have near zero or positive curvatures, indicating predominantly concave-upward terrain. In comparison, in high γ cases, most points obtain a constant negative curvature, representing convex-upward hillslopes, while the channels obtain large positive curvatures as a consequence of the steep adjacent hillslopes.

6.2 Hydromorphic balance

How can we understand the separation between channel and hillslope behavior that appears in the *DupuitLEM* model results? While there is a unique relationship between steepness and curvature for the *NoHyd* model, this is no longer the case for the *DupuitLEM* model, indicating that some information is not captured by these terms alone. The missing piece, as equation (61) shows, is Q^*. That is, there is a unique relationship between steepness, curvature, and Q^*. If we would like to know Q^*, one approach would be to solve for Q^* and explore how it could be determined from the governing equations. Using the equation for topography at steady state (20), we find Q^* as a function of the parameters, steepness, and curvature.

$$Q^* = \ell_g^{3/2} \frac{\nabla^2 z}{\sqrt{a}|\nabla z|} + \frac{h_g}{\sqrt{\ell_g}} \frac{1}{\sqrt{a}|\nabla z|} \tag{62}$$

We will call this equation the *Geomorphic Balance*. Results of plotting Q^* versus the right hand side of this equation are shown in Figure 9A. Like the relationship between steepness and curvature for the *NoHyd* model, the geomorphic balance shows a tight linear relationship. In other words, most places in the landscape have topography that is closely coupled with the runoff at that location, as predicted by the governing equations. Deviation from the 1:1 line in Figure 9A is an indication that the hydrologic state and geomorphic state are not completely in equilibrium with one another. These deviations likely have a similar origin to the perturbations in relief as the model evolves toward topographic steady state that we noted previously. Both indicate that subtle adjustments between the hydrologic and geomorphic states persist in the evolution of the modeled landscapes. This demonstration of dynamic equilibrium has similarities to natural settings where adjustment to small perturbations is persistent even in landscapes that are considered to be near geomorphic steady state.

Unfortunately in most cases where one might want to apply the *Geomorphic Balance* to real data to determine spatial patterns of runoff and saturation, the geomorphic length scales h_g and ℓ_g are unknown. While the *NoHyd* model has distinct relationships between landscape properties and h_g and ℓ_g, explored by Theodoratos et al. (2018), those relationships break down with the addition of subsurface hydrology. Even if we were to estimate h_g and ℓ_g through geomorphic methods, the uncertainty in direct estimates these parameters is likely far too great to constrain Q^* in (62).

However, the hydrologic equations offer a complementary solution for Q^*. At hydrological steady state, for steady recharge at rate p, the expression for conservation of mass (16) can be written as:

$$p = \nabla \cdot q + q_s \tag{63}$$

This should be a reasonable representation of our results, as the recharge rate is constant, and other properties vary slowly with time. Integrating this water balance over the watershed area, A, and using Leibniz' rule to evaluate the integral of the divergence term:

$$\int_A p dA = \int_A \big(\nabla \cdot q + q_s\big) dA \tag{64}$$

$$pA = \iint \nabla \cdot q \, dx dy + Q^* pA \tag{65}$$

$$pA = \oint_c q \cdot n \, dS + Q^* pA \tag{66}$$

If we assume that the catchment boundary is a no-flux boundary except for the outlet with characteristic contour width v_0, then this reduces to:

$$pA = q v_0 + Q^* pA \tag{67}$$

This also assumes that groundwater flux is directed out of the watershed, which is a tenuous assumption for deeper regional aquifers but perhaps is appropriate for the shallow near-surface aquifers that tend to produce return flow and near-channel areas of surface saturation during rainfall events. We selected the characteristic contour width v_0 here to be the same as the contour width used in (8), so the relationship $A = v_0 a$ still holds. Next we substitute the expression for groundwater flow (17). Assuming gradients are directed out of the watershed, we can take the absolute value of gradients for similarity to the geomorphic balance.

$$pA = v_0 k_s h\big(|\nabla h| + |\nabla z|\big) \cos^2(\theta) + Q^* pA \tag{68}$$

then substituting $A = a v_0$ and rearranging to solve for Q^*:

$$Q^* = 1 - \frac{k_s h}{p} \frac{\big(|\nabla h| + |\nabla z|\big) \cos^2(\theta)}{a} \tag{69}$$

By limiting ourselves to locations where the water table has reached the land surface so that the aquifer base and land surface are parallel, we can set $h \to b$ and $\nabla h \to 0$.

$$Q^* = 1 - \frac{k_s b}{p} \frac{|\nabla z| \cos^2(\theta)}{a} \tag{70}$$

This is our *Hydrologic Balance* expression for Q^*. Contained in this expression is a modified version of the topographic index $\frac{a}{\nabla z \cos^2(\theta)}$, where we have retained the cosine term for similarity to the governing equation for groundwater flow. It is appropriate that topographic index should appear in this equation, as it has been shown to be a useful tool for understanding geomorphically-driven hydrological behavior (Beven & Kirkby, 1979). The results of plotting Q^* against the right hand side of (70) are shown in Figure 9B. Correlations are not as strong as geomorphic balance. One trend that emerges is that at high drainage capacity (large γ), the fit to the theoretical curve improves as Hi increases. As discussed previously, when Hi is small, diffusive fluxes driven by gradients in aquifer thickness rather than topography are important for determining groundwater fluxes. This is something not captured in our simplified steady state model. Further investigation revealed that differences between modeled results and our analytical solution result from differences in methods of surface versus subsurface flow routing. Subsurface flow is calculated in a "diffusive" sense by measuring fluxes in or out on all links connecting nodes of the computational mesh. In contrast, surface routing is calculated with an "advective", steepest-descent approach, where all flow is routed downslope from one single node to another. The analytical solution assumes that the recharge on the up-

slope area, which we calculate with the "advective" method, is the total flow that is partitioned between surface and subsurface flow at a node. This may not always be a good assumption. Numerous unsuccessful attempts to circumvent this problem suggest that this may in fact be an intrinsic feature of a model (and perhaps reality) in which surface flow is rapid and generally channelized in a single direction, while groundwater flow is more gradual and diffusive in nature. Even with these limitations, we can continue toward a result with the analytical solution we have presented.

Now we have two expressions for Q^*: one hydrologic in (70) and one geomorphic in (62). We can combine these expressions by eliminating Q^* and obtain:

$$1 - \frac{bk_s}{p}\frac{|\nabla z|\cos^2(\theta)}{a} = \ell_g^{3/2}\frac{\nabla^2 z}{\sqrt{a}|\nabla z|} + \frac{h_g}{\sqrt{\ell_g}}\frac{1}{\sqrt{a}|\nabla z|} \tag{71}$$

or equivalently:

$$0 = \frac{bk_s}{p}\left(\frac{|\nabla z|\cos^2(\theta)}{a}\right) + \ell_g^{3/2}\left(\frac{\nabla^2 z}{\sqrt{a}|\nabla z|}\right) + \frac{h_g}{\sqrt{\ell_g}}\left(\frac{1}{\sqrt{a}|\nabla z|}\right) - 1 \tag{72}$$

We call this expression the *Hydromorphic Balance*. It describes a fundamental relationship between steepness, curvature, and topographic index that emerges from the governing equations. This relationship suggests that values of the three terms in parenthesis (which can all be calculated directly from a digital elevation model) should form a surface with linear coefficients bk_s/p, $\ell_g^{3/2}$, and $h_g/\sqrt{\ell_g}$ respectively. Using the same nondimensionalization as previously, (72) can be rewritten simply as:

$$0 = \frac{\gamma}{T_z} + \frac{C_z}{S_z} + \frac{1}{S_z} - 1 \tag{73}$$

where $T_z = \frac{\nabla' z' \cos^2(\theta)}{a'}$ is the dimensionless topographic index, $S_z = \sqrt{a'}|\nabla' z'|$ is the dimensionless steepness, and $C_z = \nabla'^2 z'$ is the dimensionless curvature. We do not expect points where $Q^* = 0$ to conform to this relationship—such as where the water table does not reach the surface—because the hydrologic component of this balance is no longer valid. An alternative way to view the components of the *Hydromorphic Balance* is in map view, separating out the terms and examining their spatial patterns. Figure 10 shows the terms of (73) for four different parameter combinations (the four corners of the space plotted in Figures 9A and 9B). The results show differing importance of terms in the low and high γ cases, with C_z/S_z more important when γ is large, and $1/S_z$ more important when γ is small. Large γ cases attain larger steepness and larger curvature than the low γ counterparts. Here we limit our scope to places where $Q^* > 0.001$. While in application, this kind of threshold would not be known, the relationship between Q^* and curvature (not shown) suggests that it would be sufficient to use the slightly more restrictive condition $\nabla^2 z > 0$ to determine areas of the landscape that should conform to the *Hydromorphic Balance*.

6.3 Emergent hillslope length

The perception that emergent length scales of the ridge-valley topography increase with drainage capacity can be quantified by measuring and comparing the average hillslope length L_h. Here, we define L_h as the mean distance from hillslope points to the nearest channel. This is inversely proportional to twice the drainage density, where drainage density is calculated with the method described by Tucker et al. (2001). Hillslope length is of particular interest in the context of hydraulic groundwater theory, where it is both an important control on hillslope storage and characteristic response time (C. Harman

& Sivapalan, 2009; Troch et al., 2003). A measure of hillslope length depends on the delineation of channel locations. While it is common to use threshold values of steepness index to identify channels (e.g., Tucker et al., 2001), this implicitly assumes a relationship between steepness and incision, which is not the case in the *DupuitLEM* model. Instead, we identify channels as points of positive Laplacian curvature ($\nabla^2 z > 0$), where fluvial incision is the dominant geomorphic process.

We can use the hydromorphic balance to predict the scaling relationship between hillslope length and the drainage capacity γ. We begin with the hydrologic and geomorphic balance expressions, equations (70) and (62). This time, rather than combining to eliminate Q^* as we did previously, we can combine to eliminate the topographic gradient $|\nabla z|$. Since we have defined channels as places where $\nabla^2 z > 0$, channel heads can be defined as places where $\nabla^2 z = 0$. We can apply the latter condition to the geomorphic balance to obtain an expression for the critical upslope area per contour width a_c at channel heads. We cannot eliminate all instances of the gradient in the hydromorphic balance, as it is present in the term $\cos(\theta) = \cos(\arctan|\nabla' z' h_g/\ell_g|)$. Here we will make the assumption that the dimensionless gradient in this term is equal to one at channel heads, such that $\cos(\theta) \approx \cos(\arctan(\alpha))$. Assuming θ is similar at channel heads across our parameter space, this assumption should only affect the coefficient scaling γ and hillslope length. We must also choose a value for Q^* in order to find a solution for both the *Hydrologic balance* and *Geomorphic Balance*, as we have not eliminated it in this case. Our results show that Q^* can vary substantially at locations of zero Laplacian curvature (not shown), but here we will introduce a constant characteristic value Q_c^* for the purposes of finding a solution. Applying these conditions, we find that the hydromorphic balance gives an expression for the area per contour width at channel heads a_c:

$$\frac{a_c}{l_g} = \left(\frac{\gamma/Q_c^{*2}}{1+\alpha^2}\right)^{2/3} \tag{74}$$

$$= \left(\frac{bk_s}{pQ_c^{*2}}\frac{h_g}{h_g^2 + l_g^2}\right)^{2/3} \tag{75}$$

or, expanding out the definitions of h_g and l_g, we can solve for the critical area at channel heads, $A_c = a_c v_0$:

$$A_c = \left(\frac{v_0 bk_s}{pQ_c^{*2}}\hat{h_g}\right)^{2/3} \tag{76}$$

where $\hat{h_g}$ is the inverse sum of two vertical length scales defined by the geomorphic variables:

$$\frac{1}{\hat{h_g}} = \frac{K}{U} + \frac{U}{\sqrt[3]{D^2 K v_0^2}} \tag{77}$$

The scaling confirms our previous observations that increasing the drainage capacity γ leads to greater spacing between channels, and therefore larger source areas at channel heads. Intuitively, this suggests that the landscape is less dissected when more flow drains through the subsurface. The expanded relationship shows a similar story: increasing $v_0 bk_s$ leads to larger contributing areas at channel heads, while increasing recharge rate p or effectiveness of fluvial incision relative to uplift lead to smaller contributing ar-

eas at channel heads. From here we further assume that the hillslope length at channel heads is proportional to the area per contour width, and thus $L_h/\ell_g \sim \gamma^{2/3}$. Despite the crudeness of this estimate, Figure 11 (left panel) shows that this scaling is in agreement with the model results when $\gamma > 1$.

7 Discussion

7.1 Hydrogeomorphic coevolution

The results presented here constitute one possible way that landscape history can be used to understand current hydrological processes by quantifying the coevolution of hydrological processes with landscape form (C. Harman & Troch, 2014; Troch et al., 2015). Prior attempts to use coevolution to understand hydrological flow paths and processes focus on evolving subsurface properties. Jefferson et al. (2010) and Yoshida and Troch (2016) explore how flow paths evolve on basaltic terrains, where porous young basalt terrains tend to drain flow vertically, while chemical weathering of basalt tends to progressively block flow paths with clays, leading to increased prevalence of lateral flow on older terrains. Both studies use space-for-time substitution to explore temporal changes in drainage density, but find contradictory trends, suggesting that underlying processes of drainage and erosion are still not well enough understood in these landscapes. Recent work on coevolution in denudational landscapes has focused on coevolution of subsurface flow paths and subsurface structure through the propagation of weathering fronts (Rempe & Dietrich, 2014; C. J. Harman & Kim, 2019; C. J. Harman & Cosans, 2019; Brantley, Lebedeva, et al., 2017). In these studies, continuous incision of streams is often used as a boundary condition to which hillslopes respond. In this study, we took a complementary approach, enforcing constant regolith thickness and permeability, while exploring surface geomorphic evolution. We found that subsurface flow plays a critical role in setting hillslope length, which may in turn affect the hydraulic gradients and flow rates that affect subsurface weathering processes. These results are consistent with the negative relationship between transmissivity and drainage density presented in Carlston (1963), and the inverse relationship between drainage density and hydraulic conductivity in the High Plains Aquifer measured by Luo and Pederson (2012). Approaches focused on surface and subsurface may be unified to formulate more general theories of the evolution of denudational landscapes.

7.2 Scaling and typology of landscapes

Our similarity approach expands upon the analysis of Theodoratos et al. (2018) and Bonetti et al. (2020). The analysis conducted by Theodoratos et al. (2018) showed that by selecting appropriate length and time scales, a standard form of the streampower-linear diffusion LEM—which uses A rather than a and does not consider an incision threshold or runoff coefficient—was parameterless, and thus had only a single landscape typology—assessed on the basis of topography—that could be rescaled to obtain every result the model could produce. As pointed out by Bonetti et al. (2020), the streampower-linear diffusion LEM does have an additional parameter, which is unaccounted for in Theodoratos et al. (2018) because the authors do not expose the differential equation that defines the upslope area per contour width. With this equation expressed, Bonetti et al. (2020) develop a nondimensionalization where one parameter remains, similar to the Peclet number that appears in Perron et al. (2008). Our analysis of the streampower-linear diffusion LEM (called the *NoHyd* model here) shows that a parameterless set of equations can still be obtained from the governing equations when accounting for the upslope area differential equation. We show that, contrary to Bonetti et al. (2020), there is a single typology for the *NoHyd* model, which can be rescaled to obtain all results the model may produce.

We develop the scaling analysis further by including the effects of runoff generated from shallow unconfined groundwater flow. This introduces four dimensionless parameters, of which three are important for the emergent topography. With this model, there is no longer a single landscape typology, but variation in form dependent on how flow is partitioned between surface and subsurface γ, the degree to which topography drives groundwater flow Hi, and the landscape gradient generated by underlying geomorphic processes α. Other typologies can certainly be imagined by the addition of other geomorphic or hydrologic processes, including a channel incision threshold (Theodoratos & Kirchner, 2020a). However the one we present is unique in that it expresses feedbacks between hydrologic and geomorphic processes, which consequently link landscape typology to hydrologic function.

7.3 Characteristic contour width and valley transmissivity

We first introduced the concept of a characteristic contour width v_0 in order to write the channel scaling relationship (Equation 7) in terms of upslope area per contour width a rather than upslope area A. This proved useful in subsequent scaling analyses, where we developed a new parameterless scaling of the governing geomorphic equations that is only possible because we have accounted for v_0 in our definitions of the geomorphic length, height, and timescales ℓ_g, h_g, and t_g. We noted previously there that we are free to choose a value of v_0, as there will always be a corresponding value of k_w to satisfy the relationship between w and a. What then is a physically meaningful characteristic contour width, and how would we identify it outside of the context of a landscape evolution model? One possible explanation appears in the hydromorphic balance equation (76) for the upslope area at channel heads, A_c. Here the characteristic contour width appears in the numerator $v_0 b k_s$, which is effectively the transmissivity integrated across a characteristic contour width. This integrated transmissivity is particularly important at channel heads, where relative magnitudes of surface and subsurface flow are similar. Upstream of the channel head, the contour width is less important, as topographic features do not constrict groundwater flow to a fixed width. Further downstream from the channel head, groundwater flow is constricted by the valley width, but most of the discharge will be transmitted as surface water rather than groundwater. Because A_c scales with v_0 just as it does with the transmissivity bk_s, v_0 plays a critical role in determining the extent of landscape dissection, as increasing channel head source areas increases the distance from channels to ridges. In landscapes similar to those modeled here, we suggest that the characteristic contour width is best thought of as characteristic channel head width, and that more attention should be paid to this factor in field investigations.

7.4 Landscape complexity

In developing this first systematic exploration of the effects of subsurface flow on steady state landscape form, we have neglected the complexity of landscape processes and heterogeneity of landscape properties in favor of an approach with a tractable number of parameters so that we can explore the diversity of behaviors it can produce. However, it is likely that processes and heterogeneity not captured here have significant impacts on landscape form. Subsurface properties are not only heterogeneous, but spatially organized, including systematic variations in permeability with depth through soil and weathered bedrock and along hillslope catenas (Lohse & Dietrich, 2005). The scope of runoff generation processes we have examined is also limited, as we have not considered infiltration excess overland flow, nor other erosional processes that are linked to shallow groundwater, including seepage erosion (Abrams et al., 2009; Laity & Malin, 1985) and landsliding driven by excess pore water pressure (Montgomery & Dietrich, 1994). Likewise, ecological processes may act on the environment in ways that cannot be captured by the processes and parameters included here. For example, feedback between depth to water table and tree growth may affect spatial patterns of hillslope and fluvial sed-

iment transport, as trees anchor sediment with roots, displace sediment through treethrow, or encourage soil production (Brantley, Eissenstat, et al., 2017; Gabet & Mudd, 2010).

7.5 Steady state topography

In this study we have focused on evaluating landscapes near topographic steady state in order to understand the emergent relationships between topography and hydrology generated by these governing equations. This is a powerful method employed in landscape evolution models to understand the form toward which landscapes will evolve (e.g., Perron et al., 2008; Theodoratos et al., 2018). In the model we have used here, however, times to steady state are long (millions to tens of millions of years) compared to real timescales of variability in climate and baselevel change. For this reason, transience, at least in some portions of the landscape, is likely the norm in real landscapes with similar dominant processes to those modeled here (Whipple, 2001). On the other hand, nonlinear models of hillslope diffusion show substantially shorter times to steady state (Roering et al., 2001), which may be important when hillslopes are the limiting factor in reaching topographic steady state. Further investigation could focus on transient responses the model considered here, which may provide insights into a wider range of humid landscapes.

7.6 Steady recharge

In this model, we have shown that runoff generation from shallow groundwater driven by steady recharge has a strong effect on emergent landscape properties. With increasing γ, we found that the hydrological function of the landscape was increasingly binary: channels have surface runoff nearly equal to the sum of the recharge on the area upslope, while hillslopes do not contribute surface runoff at all. While this may be characteristic of some landscapes where saturated areas are more or less constant in time, in many places, saturated areas and wetted channels expand and contract in response to the arrival of storm events or snow melt (Dunne & Black, 1970; Nippgen et al., 2015; Antonelli et al., 2020). Furthermore, antecedent wetness plays an important role in determining the hydrological response to precipitation (Longobardi et al., 2003; O'Loughlin, 1981). As fluvial sediment transport in our model is proportional to runoff Q^*, we expect that precipitation stochasticity and subsurface water storage affect sediment transport and thus ultimately will affect the landscape form as well. Previous studies have shown that landscape form and channel profiles have are sensitive to variability in precipitation or discharge, depending on factors including the presence of erosion thresholds and the nonlinearity of the fluvial incision model (Tucker, 2004; Lague et al., 2005; Deal et al., 2018). In a future contribution, we will extend the theoretical framework used here to incorporate stochastic precipitation, allowing allowing us to explore the emergence of hydrogeomorphic features such as variable source areas.

8 Conclusion

Here we have coupled a model of shallow groundwater flow with a model of denudational landscape evolution, and have shown the first results of such a model at topographic steady state. The shallow aquifer model uses the Dupuit-Forcheimer assumptions to generate lateral groundwater flow and surface water discharge from groundwater return flow and precipitation on saturated areas. The topography evolves according to fluvial incision by routed flow generated by the groundwater model, linear hillslope diffusion, and a constant rate of uplift. We use a novel scaling analysis to guide or numerical simulations, and find that the subsurface drainage capacity relative to climate plays a critical role in setting topographic properties including hillslope length. We showed that the linear relationship between steepness and Laplacian curvature that emerges from the simple streampower incision-linear diffusion LEM bifurcates with increasing subsurface drainage capacity: saturated areas tend toward the linear relationship between steepness and cur-

vature, while unsaturated hillslopes maintain constant negative curvature regardless of steepness. By incorporating the steady state solution of the hydrological model, we can explain the model results not as falling along a line of steepness and curvature, but as sitting on a manifold that relates steepness, Laplacian curvature, and topographic index. A complementary analysis of the governing equations at steady state showed that hillslope length should scale with the subsurface drainage capacity, and therefore the transmissivity, to the power 2/3. This was supported by our numerical results for sufficiently large drainage capacities. This analysis provides a pathway toward estimating subsurface transmissivity at the landscape scale using terrain analysis. Links between landscape form and hydrologic function have been long sought-after in hydrology. Our work examines the possibility that an understanding of landscape history through the coevolution of landforms and hydrological process could be useful for generating hypotheses about these relationships that can be tested against field data. If successful, this approach could complement existing approaches for estimating hydrological parameters across regions or continents that are often necessary to drive large scale hydrological and land surface models.

9 Notation

Variable definitions are below, with dimensions length L, time T, and mass M. Prime always indicates the dimensionless equivalent, where dimensionless equivalents are defined in the text.

variable	name	dimension
x, y	horizontal coordinates	$[L]$
t	time	$[T]$
$z(x, y)$	topographic elevation	$[L]$
$h(x, y)$	aquifer thickness	$[L]$
$A(x, y)$	area upslope	$[L^2]$
$a(x, y)$	area upslope per unit contour width	$[L]$
$\theta(x, y)$	aquifer base slope angle	$[rad]$
h_g	characteristic geomorphic height scale	$[L]$
ℓ_g	characteristic geomorphic length scale	$[L]$
t_g	characteristic geomorphic time scale	$[T]$
h_c	characteristic hydrologic height scale	$[L]$
t_d	characteristic time to drain aquifer storage	$[T]$
E_f	fluvial incision rate	$[L/T]$
E_h	hillslope diffusion rate	$[L/T]$
U	uplift rate	$[L/T]$
K	streampower incision coefficient	$[1/T]$
m	streampower area exponent	$[-]$
n	streampower slope exponent	$[-]$
v_0	characteristic contour width	[L]
τ	bed shear stress	$[M/LT^2]$
τ_c	critical bed shear stress	$[M/LT^2]$
k_e	erosivity coefficient	$[M^{-\beta}L^{1+\beta}T^{2\beta-1}]$
β	shear stress exponent	$[-]$
ρ_w	density of water	$[M/L^3]$
g	acceleration due to gravity	$[L/T^2]$
d_f	channel flow depth	$[L]$
C	Chezy coefficient	$[L^{1/2}/T]$
w	channel width	$[L]$
k_w	width coefficient	$[-]$
b	permeable thickness	$[L]$
q_h	hillslope sediment transport rate	$[L^2/T]$
D	hillslope diffusivity	$[L^2/T]$
k_{sf}	timestep scaling factor	$[-]$
$q(x, y, t)$	groundwater specific discharge	$[L^2/T]$
$q_s(x, y, t)$	local surface runoff	$[L/T]$
$Q(x, y, t)$	discharge	$[L^3/T]$
$Q^*(x, y, t)$	dimensionless discharge	$[-]$
p	recharge rate	$[L/T]$
k_s	hydraulic conductivity	$[L/T]$
n	drainable porosity	$[-]$
$\mathcal{G}$	step function	
$\mathcal{R}$	ramp function	

Acknowledgments

This work was supported by NSF grants EAR-2012264, EAR-1654194, ACI-1450409, EAR-1725774, and EAR-1831623. No original data is presented in this paper. The code used here is archived at `https://doi.org/10.5281/zenodo.4727916`. Model output files will be archived and available prior to final publication.

References

Abrams, D. M., Lobkovsky, A. E., Petroff, A. P., Straub, K. M., McElroy, B., Mohrig, D. C., ... Rothman, D. H. (2009, March). Growth laws for channel networks incised by groundwater flow. *Nature Geoscience*, *2*(3), 193–196. Retrieved 2019-11-11, from http://www.nature.com/articles/ngeo432 doi: 10.1038/ngeo432

Ahnert, F. (1976). Brief description of a comprehensive three-dimensional process-response model of landform development. *Zeitschrift für Geomorphologie, Supplement*, *25*, 29–49.

Antonelli, M., Glaser, B., Teuling, A. J., Klaus, J., & Pfister, L. (2020, March). Saturated areas through the lens: 1. Spatio-temporal variability of surface saturation documented through thermal infrared imagery. *Hydrological Processes*, *34*(6), 1310–1332. Retrieved 2021-03-26, from https://onlinelibrary.wiley.com/doi/abs/10.1002/hyp.13698 doi: 10.1002/hyp.13698

Armstrong, A. (1976). A three-dimensional simulation of slope forms. *Zeitschrift für Geomorphologie, Supplement*, *25*, 20–28.

Barenblatt, G. I. (1996). *Scaling, self-similarity, and intermediate asymptotics* (No. 14). Cambridge ; New York: Cambridge University Press.

Barnhart, K. R., Hutton, E. W. H., Tucker, G. E., Gasparini, N. M., Istanbulluoglu, E., Hobley, D. E. J., ... Bandaragoda, C. (2020, May). Short communication: Landlab v2.0: a software package for Earth surface dynamics. *Earth Surface Dynamics*, *8*(2), 379–397. Retrieved 2020-11-27, from https://esurf.copernicus.org/articles/8/379/2020/ (Publisher: Copernicus GmbH) doi: https://doi.org/10.5194/esurf-8-379-2020

Barnhart, K. R., Tucker, G. E., Doty, S. G., Glade, R. C., Shobe, C. M., Rossi, M. W., & Hill, M. C. (2020). Projections of Landscape Evolution on a 10,000 Year Timescale With Assessment and Partitioning of Uncertainty Sources. *Journal of Geophysical Research: Earth Surface*, *125*(12), e2020JF005795. Retrieved 2021-01-05, from http://agupubs.onlinelibrary.wiley.com/doi/abs/10.1029/2020JF005795 (_eprint: https://onlinelibrary.wiley.com/doi/pdf/10.1029/2020JF005795) doi: https://doi.org/10.1029/2020JF005795

Barnhart, K. R., Tucker, G. E., Doty, S. G., Shobe, C. M., Glade, R. C., Rossi, M. W., & Hill, M. C. (2020). Inverting Topography for Landscape Evolution Model Process Representation: 3. Determining Parameter Ranges for Select Mature Geomorphic Transport Laws and Connecting Changes in Fluvial Erodibility to Changes in Climate. *Journal of Geophysical Research: Earth Surface*, *125*(7), e2019JF005287. Retrieved 2020-07-08, from http://agupubs.onlinelibrary.wiley.com/doi/abs/10.1029/2019JF005287 (_eprint: https://onlinelibrary.wiley.com/doi/pdf/10.1029/2019JF005287) doi: 10.1029/2019JF005287

Beven, K. J., & Kirkby, M. J. (1979). A physically based, variable contributing area model of basin hydrology. *Hydrological Sciences Bulletin*, *24*(1), 43–69. (ISBN: 0262666790) doi: 10.1080/02626667909491834

Bishop, P. (2007). Long-term landscape evolution: linking tectonics and surface processes. *Earth Surface Processes and Landforms*, *32*(3), 329–365. Retrieved 2021-04-11, from http://onlinelibrary.wiley.com/doi/abs/10.1002/esp.1493 (_eprint: https://onlinelibrary.wiley.com/doi/pdf/10.1002/esp.1493) doi: https://doi.org/10.1002/esp.1493

Bonetti, S., Bragg, A. D., & Porporato, A. (2018, March). On the theory of drainage area for regular and non-regular points. *Proceedings of the Royal Society A: Mathematical, Physical and Engineering Sciences*, *474*(2211), 20170693. Retrieved 2021-01-13, from https://royalsocietypublishing.org/doi/full/10.1098/rspa.2017.0693 (Publisher: Royal Society) doi: 10.1098/rspa.2017.0693

Bonetti, S., Hooshyar, M., Camporeale, C., & Porporato, A. (2020, January). Channelization cascade in landscape evolution. *Proceedings of the National Academy of Sciences*, *117*(3), 1375–1382. Retrieved 2020-12-02, from https://www.pnas.org/content/117/3/1375 (Publisher: National Academy of Sciences Section: Physical Sciences) doi: 10.1073/pnas.1911817117

Brantley, S. L., Eissenstat, D. M., Marshall, J. A., Godsey, S. E., Balogh-Brunstad, Z., Karwan, D. L., ... Weathers, K. C. (2017). Reviews and syntheses: On the roles trees play in building and plumbing the critical zone. *Biogeosciences*, *14*(22), 5115–5142. doi: 10.5194/bg-14-5115-2017

Brantley, S. L., Lebedeva, M. I., Balashov, V. N., Singha, K., Sullivan, P. L., & Stinchcomb, G. (2017, January). Toward a conceptual model relating chemical reaction fronts to water flow paths in hills. *Geomorphology*, *277*, 100–117. Retrieved 2019-11-13, from https://linkinghub.elsevier.com/retrieve/pii/S0169555X16308674 doi: 10.1016/j.geomorph.2016.09.027

Braun, J., & Willett, S. D. (2013). A very efficient O(n), implicit and parallel method to solve the stream power equation governing fluvial incision and landscape evolution. *Geomorphology*, *180-181*, 170–179. Retrieved from http://dx.doi.org/10.1016/j.geomorph.2012.10.008 doi: 10.1016/j.geomorph.2012.10.008

Brocca, L., Melone, F., Moramarco, T., & Singh, V. P. (2009, February). Assimilation of Observed Soil Moisture Data in Storm Rainfall-Runoff Modeling. *Journal of Hydrologic Engineering*, *14*(2), 153–165. doi: 10.1061/(ASCE)1084-0699(2009)14:2(153)

Brutsaert, W. (2005). *Hydrology: An Introduction*. Cambridge University Press. Retrieved from https://books.google.com/books?id=yX_xS55xxyoC

Carlston, C. W. (1963). *Drainage density and streamflow*. U.S. Govt. Print. Off. (Google-Books-ID: FLsvAAAAYAAJ)

Chen, A., Darbon, J., & Morel, J.-M. (2014, August). Landscape evolution models: A review of their fundamental equations. *Geomorphology*, *219*, 68–86. Retrieved 2020-12-03, from http://www.sciencedirect.com/science/article/pii/S0169555X14002402 doi: 10.1016/j.geomorph.2014.04.037

Childs, E. C. (1971). Drainage of Groundwater Resting on a Sloping Bed. *Water Resources Research*, *7*(5), 1256–1263. Retrieved 2019-11-11, from https://agupubs.onlinelibrary.wiley.com/doi/abs/10.1029/WR007i005p01256 doi: 10.1029/WR007i005p01256

Deal, E., Braun, J., & Botter, G. (2018). Understanding the Role of Rainfall and Hydrology in Determining Fluvial Erosion Efficiency. *Journal of Geophysical Research: Earth Surface*, *123*(4), 744–778. doi: 10.1002/2017JF004393

Dietrich, W. E., Bellugi, D. G., Sklar, L. S., Stock, J. D., Heimsath, A. M., & Roering, J. J. (2003). Geomorphic Transport Laws for Predicting Landscape form and Dynamics. In P. R. Wilcock & R. M. Iverson (Eds.), *Geophysical Monograph Series* (pp. 103–132). Washington, D. C: American Geophysical Union. Retrieved 2021-02-09, from http://doi.wiley.com/10.1029/135GM09 doi: 10.1029/135GM09

Dietrich, W. E., Wilson, C. J., Montgomery, D. R., & McKean, J. (1993, March). Analysis of Erosion Thresholds, Channel Networks, and Landscape Morphology Using a Digital Terrain Model. *The Journal of Geology*, *101*(2), 259–278. Retrieved 2021-04-09, from https://www.journals.uchicago.edu/doi/abs/10.1086/648220 (Publisher: The University of Chicago Press) doi: 10.1086/648220

Dunne, T. (1978). Field studies of hillslope flow processes. In *Hillslope Hydrology*.

Dunne, T., & Black, R. D. (1970). Partial Area Contributions to Storm Runoff in a Small New England Watershed. *Water Resources Research*, *6*(5), 1296–1311. (ISBN: 0043-1397) doi: 10.1029/WR006i005p01296

Forte, A. M., Yanites, B. J., & Whipple, K. X. (2016). Complexities of landscape

evolution during incision through layered stratigraphy with contrasts in rock strength. *Earth Surface Processes and Landforms*, *41*(12), 1736–1757. Retrieved 2020-01-20, from https://onlinelibrary.wiley.com/doi/abs/10.1002/esp.3947 doi: 10.1002/esp.3947

Gabet, E. J., & Mudd, S. M. (2009). A theoretical model coupling chemical weathering rates with denudation rates. *Geology*, *37*(2), 151–154. doi: 10.1130/G25270A.1

Gabet, E. J., & Mudd, S. M. (2010). Bedrock erosion by root fracture and tree throw: A coupled biogeomorphic model to explore the humped soil production function and the persistence of hillslope soils. *Journal of Geophysical Research: Earth Surface*, *115*(F4). Retrieved 2020-01-10, from https://agupubs.onlinelibrary.wiley.com/doi/abs/10.1029/2009JF001526 doi: 10.1029/2009JF001526

Harman, C., & Sivapalan, M. (2009). A similarity framework to assess controls on shallow subsurface flow dynamics in hillslopes. *Water Resources Research*, *45*(1), 1–12. doi: 10.1029/2008WR007067

Harman, C., & Troch, P. A. (2014, February). What makes Darwinian hydrology "Darwinian"? Asking a different kind of question about landscapes. *Hydrology and Earth System Sciences*, *18*(2), 417–433. Retrieved 2020-01-22, from https://www.hydrol-earth-syst-sci.net/18/417/2014/ doi: 10.5194/hess-18-417-2014

Harman, C. J., & Cosans, C. L. (2019). A low-dimensional model of bedrock weathering and lateral flow coevolution in hillslopes: 2. Controls on weathering and permeability profiles, drainage hydraulics, and solute export pathways. *Hydrological Processes*(December 2018), 1168–1190. doi: 10.1002/hyp.13385

Harman, C. J., & Kim, M. (2019). A low-dimensional model of bedrock weathering and lateral flow coevolution in hillslopes: 1. Hydraulic theory of reactive transport. *Hydrological Processes*, *33*(4), 466–475. Retrieved from https://onlinelibrary.wiley.com/doi/pdf/10.1002/hyp.13360 doi: 10.1002/hyp.13360

Hewlett, J. D., & Hibbert, A. R. (1967). Factors affecting the response of small watersheds to precipitation in humid areas. In *Int. Symp. Forest Hydrology.* doi: 10.1177/0309133309338118

Hobley, D. E. J., Adams, J. M., Nudurupati, S. S., Hutton, E. W. H., Gasparini, N. M., Istanbulluoglu, E., & Tucker, G. E. (2017). Creative computing with Landlab: an open-source toolkit for building, coupling, and exploring two-dimensional numerical models of Earth-surface dynamics. , 21–46. doi: 10.5194/esurf-5-21-2017

Horton, R. E. (1945, March). Erosional development of streams and their drainage basins; hydrophysical approach to quantitative morphology. *GSA Bulletin*, *56*(3), 275–370. Retrieved from https://doi.org/10.1130/0016-7606(1945)56[275:EDOSAT]2.0.CO doi: 10.1130/0016-7606(1945)56[275:EDOSAT]2.0.CO;2

Howard, A. D. (1994). A detachment-limited model of drainage basin evolution. *Water Resources Research*, *30*(7), 2261–2285. Retrieved 2020-01-16, from https://agupubs.onlinelibrary.wiley.com/doi/abs/10.1029/94WR00757 doi: 10.1029/94WR00757

Howard, A. D., & Kerby, G. (1983, June). Channel changes in badlands. *GSA Bulletin*, *94*(6), 739–752. Retrieved 2020-01-20, from https://pubs.geoscienceworld.org/gsabulletin/article/94/6/739/202874/Channel-changes-in-badlands doi: 10.1130/0016-7606(1983)94⟨739:CCIB⟩2.0.CO;2

Huang, X., & Niemann, J. D. (2006). Modelling the potential impacts of groundwater hydrology on long-term drainage basin evolution. *Earth Surface Processes and Landforms*. doi: 10.1002/esp.1369

Huang, X., & Niemann, J. D. (2008). How do streamflow generation mechanisms affect watershed hypsometry? *Earth Surface Processes and Landforms*. doi: 10.1002/esp.1573

Ijjász-Vásquez, E. J., Bras, R. L., & Moglen, G. E. (1992). Sensitivity of a basin evolution model to the nature of runoff production and to initial conditions. doi: 10.1029/92WR01561

Jefferson, A., Grant, G. E., Lewis, S. L., & Lancaster, S. T. (2010). Coevolution of hydrology and topography on a basalt landscape in the Oregon Cascade Range, USA. *Earth Surface Processes and Landforms*, *35*(7), 803–816. doi: 10.1002/esp.1976

Lague, D., Hovius, N., & Davy, P. (2005, December). Discharge, discharge variability, and the bedrock channel profile. *Journal of Geophysical Research: Earth Surface*, *110*(F4). Retrieved 2021-03-18, from `http://agupubs.onlinelibrary.wiley.com/doi/full/10.1029/2004JF000259` (Publisher: John Wiley & Sons, Ltd) doi: 10.1029/2004JF000259

Laity, J. E., & Malin, M. C. (1985). Sapping processes and the development of theater-headed valley networks on the Colorado Plateau. *Geological Society of America Bulletin*, *96*, 203–217.

Lapides, D. A., David, C., Sytsma, A., Dralle, D., & Thompson, S. (2020, August). Analytical Solutions To Runoff On Hillslopes With Curvature: Numerical And Laboratory Verification. *Hydrological Processes*, hyp.13879. Retrieved 2020-08-15, from `https://onlinelibrary.wiley.com/doi/abs/10.1002/hyp.13879` doi: 10.1002/hyp.13879

Leopold, L. B., & Maddock, T. (1953). *The Hydraulic Geometry of Stream Channels and Some Physiographic Implications*. U.S. Government Printing Office. (Google-Books-ID: 4UGH22BKfdsC)

Litwin, D., Tucker, G., Barnhart, K., & Harman, C. (2020, February). GroundwaterDupuitPercolator: A Landlab component for groundwater flow. *Journal of Open Source Software*, *5*(46), 1935. Retrieved 2020-02-11, from `https://joss.theoj.org/papers/10.21105/joss.01935` doi: 10.21105/joss.01935

Lohse, K. A., & Dietrich, W. E. (2005). Contrasting effects of soil development on hydrological properties and flow paths. *Water Resources Research*, *41*(12), 1–17. doi: 10.1029/2004WR003403

Longobardi, A., Villani, P., Grayson, R. B., & Western, A. W. (2003). On the relationship between runoff coefficient and catchment initial conditions. *Modelling and Simulation Society of Australia and New Zealand*, *2*(1), 1–6. (ISBN: 1-74052-098-X)

Luo, W., & Pederson, D. T. (2012). Hydraulic conductivity of the High Plains Aquifer re-evaluated using surface drainage patterns. *Geophysical Research Letters*, *39*(2). Retrieved 2021-04-11, from `http://agupubs.onlinelibrary.wiley.com/doi/abs/10.1029/2011GL050200` (_eprint: https://onlinelibrary.wiley.com/doi/pdf/10.1029/2011GL050200) doi: https://doi.org/10.1029/2011GL050200

Martin, Y., & Church, M. (2004, September). Numerical modelling of landscape evolution: geomorphological perspectives. *Progress in Physical Geography: Earth and Environment*, *28*(3), 317–339. Retrieved 2021-04-11, from `https://doi.org/10.1191/0309133304pp412ra` (Publisher: SAGE Publications Ltd) doi: 10.1191/0309133304pp412ra

Marçais, J., de Dreuzy, J. R., & Erhel, J. (2017). Dynamic coupling of subsurface and seepage flows solved within a regularized partition formulation. *Advances in Water Resources*, *109*, 94–105. doi: 10.1016/j.advwatres.2017.09.008

Montgomery, D. R., & Dietrich, W. E. (1994, April). A physically based model for the topographic control on shallow landsliding. *Water Resources Research*, *30*(4), 1153–1171. Retrieved 2021-02-02, from `http://agupubs.onlinelibrary.wiley.com/doi/abs/10.1029/93WR02979` (Pub-

lisher: John Wiley & Sons, Ltd) doi: 10.1029/93WR02979

Nippgen, F., McGlynn, B. L., & Emanuel, R. E. (2015). The spatial and temporal evolution of contributing areas. *Water Resources Research*. doi: 10.1002/2014WR016719

O'Loughlin, E. M. (1981). Saturation regions in catchments and their relations to soil and topographic properties. *Journal of Hydrology*, *53*(3-4), 229–246. (ISBN: 0022-1694) doi: 10.1016/0022-1694(81)90003-2

Pazzaglia, F. J. (2003, January). Landscape evolution models. In *Developments in Quaternary Sciences* (Vol. 1, pp. 247–274). Elsevier. Retrieved 2021-04-11, from https://www.sciencedirect.com/science/article/pii/S1571086603010121 doi: 10.1016/S1571-0866(03)01012-1

Pelletier, J. D. (2013, January). 2.3 Fundamental Principles and Techniques of Landscape Evolution Modeling. In J. F. Shroder (Ed.), *Treatise on Geomorphology* (pp. 29–43). San Diego: Academic Press. Retrieved 2021-04-11, from https://www.sciencedirect.com/science/article/pii/B9780123747396000257 doi: 10.1016/B978-0-12-374739-6.00025-7

Perron, J. T., Dietrich, W. E., & Kirchner, J. W. (2008). Controls on the spacing of first-order valleys. *Journal of Geophysical Research: Earth Surface*, *113*(4), 1–21. doi: 10.1029/2007JF000977

Prancevic, J. P., & Kirchner, J. W. (2019). Topographic controls on the extension and retraction of flowing streams. *Geophysical Research Letters*, *0*(0). Retrieved from https://agupubs.onlinelibrary.wiley.com/doi/abs/10.1029/2018GL081799 doi: 10.1029/2018GL081799

Rempe, D. M., & Dietrich, W. E. (2014, May). A bottom-up control on fresh-bedrock topography under landscapes. *Proceedings of the National Academy of Sciences*, *111*(18), 6576–6581. Retrieved 2019-11-03, from http://www.pnas.org/cgi/doi/10.1073/pnas.1404763111 doi: 10.1073/pnas.1404763111

Roering, J. J. (2008, September). How well can hillslope evolution models "explain" topography? Simulating soil transport and production with high-resolution topographic data. *Geological Society of America Bulletin*, *120*(9-10), 1248–1262. Retrieved 2019-09-19, from https://pubs.geoscienceworld.org/gsabulletin/article/120/9-10/1248-1262/2317 doi: 10.1130/B26283.1

Roering, J. J., Kirchner, J. W., & Dietrich, W. E. (1999). Evidence for nonlinear, diffusive sediment transport on hillslopes and implications for landscape morphology. *Water Resources Research*, *35*(3), 853–870. doi: 10.1029/1998WR900090

Roering, J. J., Kirchner, J. W., & Dietrich, W. E. (2001, August). Hillslope evolution by nonlinear, slope-dependent transport: Steady state morphology and equilibrium adjustment timescales. *Journal of Geophysical Research: Solid Earth*, *106*(B8), 16499–16513. Retrieved 2021-04-20, from http://agupubs.onlinelibrary.wiley.com/doi/abs/10.1029/2001jb000323 (Publisher: John Wiley & Sons, Ltd) doi: 10.1029/2001JB000323

Rosenbloom, N. A., & Anderson, R. S. (1994, July). Hillslope and channel evolution in a marine terraced landscape, Santa Cruz, California. *Journal of Geophysical Research: Solid Earth*, *99*(B7), 14013–14029. Retrieved 2019-09-26, from https://agupubs.onlinelibrary.wiley.com/doi/10.1029/94JB00048@10.1002/(ISSN)2169-9356.TECTOP1 doi: 10.1029/94JB00048@10.1002/(ISSN)2169-9356.TECTOP1

Snyder, N. P., Whipple, K. X., Tucker, G. E., & Merritts, D. J. (2003, July). Channel response to tectonic forcing: field analysis of stream morphology and hydrology in the Mendocino triple junction region, northern California. *Geomorphology*, *53*(1), 97–127. Retrieved 2021-04-21, from https://www.sciencedirect.com/science/article/pii/S0169555X02003495 doi: 10.1016/S0169-555X(02)00349-5

Tarboton, D. G., Bras, R. L., & Rodriguez-Iturbe, I. (1989, September). Scaling and elevation in river networks. *Water Resources Research*, *25*(9), 2037–2051. Retrieved 2021-04-09, from http://agupubs.onlinelibrary.wiley.com/doi/abs/10.1029/WR025i009p02037 (Publisher: John Wiley & Sons, Ltd) doi: 10.1029/WR025i009p02037

Temme, A. J. A. M., Schoorl, J. M., Claessens, L., & Veldkamp, A. (2013, January). 2.13 Quantitative Modeling of Landscape Evolution. In J. F. Shroder (Ed.), *Treatise on Geomorphology* (pp. 180–200). San Diego: Academic Press. doi: 10.1016/B978-0-12-374739-6.00039-7

Theodoratos, N., & Kirchner, J. W. (2020a, June). Dimensional analysis of a landscape evolution model with incision threshold. *Earth Surface Dynamics*, *8*(2), 505–526. Retrieved 2020-06-04, from https://www.earth-surf-dynam.net/8/505/2020/ (Publisher: Copernicus GmbH) doi: https://doi.org/10.5194/esurf-8-505-2020

Theodoratos, N., & Kirchner, J. W. (2020b, June). Graphically interpreting how incision thresholds influence topographic and scaling properties of modeled landscapes. *Earth Surface Dynamics Discussions*, 1–25. Retrieved 2021-04-15, from https://esurf.copernicus.org/preprints/esurf-2020-45/ (Publisher: Copernicus GmbH) doi: 10.5194/esurf-2020-45

Theodoratos, N., Seybold, H., & Kirchner, J. W. (2018, September). Scaling and similarity of a stream-power incision and linear diffusion landscape evolution model. *Earth Surface Dynamics*, *6*(3), 779–808. Retrieved 2020-08-03, from https://esurf.copernicus.org/articles/6/779/2018/ (Publisher: Copernicus GmbH) doi: https://doi.org/10.5194/esurf-6-779-2018

Tramblay, Y., Bouvier, C., Martin, C., Didon-Lescot, J.-F., Todorovik, D., & Domergue, J.-M. (2010, June). Assessment of initial soil moisture conditions for event-based rainfall–runoff modelling. *Journal of Hydrology*, *387*(3), 176–187. Retrieved 2020-01-08, from http://www.sciencedirect.com/science/article/pii/S0022169410001873 doi: 10.1016/j.jhydrol.2010.04.006

Troch, P. A., Lahmers, T., Meira, A., Mukherjee, R., Pedersen, J. W., Roy, T., & Valdes-Pineda, R. (2015). Catchment coevolution: A useful framework for improving predictions of hydrological change? *Water Resources Research*, *51*(7), 4903–4922. (arXiv: 10.1002/2014WR016527 ISBN: 6176273099) doi: 10.1002/2015WR017032

Troch, P. A., Paniconi, C., & Van Loon, E. E. (2003). Hillslope-storage Boussinesq model for subsurface flow and variable source areas along complex hillslopes: 1. Formulation and characteristic response. *Water Resources Research*, *39*(11). doi: 10.1029/2002WR001728

Tsujimoto, T. (1999). Sediment transport processes and channel incision: mixed size sediment transport, degradation and armoring. *Incised river channels*, 37–66. (Publisher: John Wiley Hoboken, NJ)

Tucker, G. E. (2004). Drainage basin sensitivity to tectonic and climatic forcing: implications of a stochastic model for the role of entrainment and erosion thresholds. *Earth Surface Processes and Landforms*, *29*(2), 185–205. Retrieved 2020-01-20, from https://onlinelibrary.wiley.com/doi/abs/10.1002/esp.1020 doi: 10.1002/esp.1020

Tucker, G. E., & Bras, R. L. (1998). Hillslope processes, drainage density, and landscape morphology. *Water Resources Research*, *34*(10), 2751–2764. Retrieved from http://doi.wiley.com/10.1029/98WR01474 doi: 10.1029/98WR01474

Tucker, G. E., Catani, F., Rinaldo, A., & Bras, R. L. (2001, February). Statistical analysis of drainage density from digital terrain data. *Geomorphology*, *36*(3), 187–202. Retrieved 2019-09-25, from http://www.sciencedirect.com/science/article/pii/S0169555X00000568 doi: 10.1016/S0169-555X(00)00056-8

Tucker, G. E., & Slingerland, R. (1997). Drainage basin responses to climate change. *Water Resources Research*, *33*(8), 2031–2047. Retrieved 2020-01-09, from https://agupubs.onlinelibrary.wiley.com/doi/abs/10.1029/97WR00409 doi: 10.1029/97WR00409

Valters, D. (2016, May). Modelling Geomorphic Systems: Landscape Evolution. In (p. 6.5.12). doi: 10.13140/RG.2.1.1970.9047

West, A. J., Galy, A., & Bickle, M. (2005, June). Tectonic and climatic controls on silicate weathering. *Earth and Planetary Science Letters*, *235*(1), 211–228. Retrieved 2021-02-10, from https://www.sciencedirect.com/science/article/pii/S0012821X05002116 doi: 10.1016/j.epsl.2005.03.020

Whipple, K. X. (2001, April). Fluvial Landscape Response Time: How Plausible Is Steady-State Denudation? *American Journal of Science*, *301*(4-5), 313–325. Retrieved 2021-01-11, from https://www.ajsonline.org/content/301/4-5/313 (Publisher: American Journal of Science Section: ARTICLES) doi: 10.2475/ajs.301.4-5.313

Whipple, K. X., Hancock, G. S., & Anderson, R. S. (2000). River incision into bedrock: Mechanics and relative efficacy of plucking, abrasion and cavitation. *Geological Society of America Bulletin*, 18.

Whipple, K. X., & Tucker, G. E. (1999). Dynamics of the stream-power river incision model: Implications for height limits of mountain ranges, landscape response timescales, and research needs. *Journal of Geophysical Research: Solid Earth*, *104*(B8), 17661–17674. Retrieved 2019-11-03, from https://agupubs.onlinelibrary.wiley.com/doi/abs/10.1029/1999JB900120 doi: 10.1029/1999JB900120

Willgoose, G., Bras, R. L., & Rodriguez-Iturbe, I. (1991, July). A physical explanation of an observed link area-slope relationship. *Water Resources Research*, *27*(7), 1697–1702. Retrieved 2021-04-09, from http://agupubs.onlinelibrary.wiley.com/doi/abs/10.1029/91WR00937 (Publisher: John Wiley & Sons, Ltd) doi: 10.1029/91WR00937

Willgoose, G., Bras, R. L., & Rodriguez-Iturbe, I. (1991). A coupled channel network growth and hillslope evolution model: 1. Theory. *Water Resources Research*, 1671–1684. doi: 10.1029/91WR00935@10.1002/(ISSN)1944-7973.USALPINE1

Wohl, E., & David, G. C. L. (2008). Consistency of scaling relations among bedrock and alluvial channels. *Journal of Geophysical Research: Earth Surface*, *113*(F4). Retrieved 2021-04-09, from http://agupubs.onlinelibrary.wiley.com/doi/abs/10.1029/2008JF000989 doi: https://doi.org/10.1029/2008JF000989

Yoshida, T., & Troch, P. A. (2016). Coevolution of volcanic catchments in Japan. *Hydrology and Earth System Sciences*, *20*(3), 1133–1150. (ISBN: 1607-7938) doi: 10.5194/hess-20-1133-2016

Zhang, Y., Slingerland, R., & Duffy, C. (2016). Fully-coupled hydrologic processes for modeling landscape evolution. *Environmental Modelling and Software*, *82*, 89–107. Retrieved from http://dx.doi.org/10.1016/j.envsoft.2016.04.014 doi: 10.1016/j.envsoft.2016.04.014

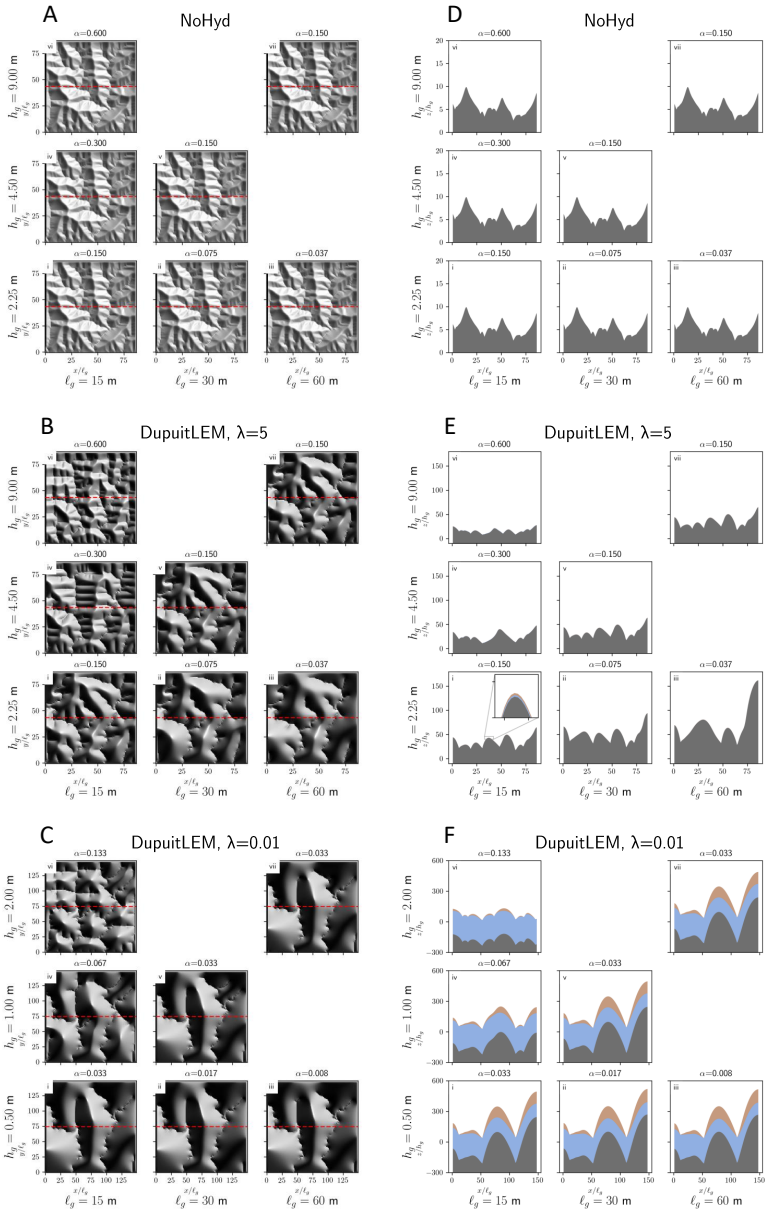

Figure 1. Hillshade plots (A, B, C) and cross sections (D, E, F) of steady state elevation for model runs with varying h_g and ℓ_g. Cross sections are taken along the dashed red lines. Data plotted are in the re-scaled coordinate system (x', y', z'). (A, D) Model runs with the *NoHyd* model, showing topography is nearly identical between the runs in the dimensionless coordinate system regardless of the chosen values of h_g and ℓ_g. (B, E) *DupuitLEM* model results are sensitive to independent scaling of ℓ_g $(i \rightarrow ii \rightarrow iii)$ and h_g $(i \rightarrow iv \rightarrow vi)$ when Hi is large. Scaling such that $\alpha = h_g/\ell_g$ remains constant produces topography that is similar in the re-scaled coordinates. (C, F) *DupuitLEM* results with small Hi, showing reduced sensitivity of modeled topography to chosen length scales for small values of α. Note that the dimensionless size of the domain in the Hi $=$ 0.01 cases is larger than the other cases in order to resolve a sufficient number of ridge-valley features. This was accomplished by maintaining the number of grid cells and increasing the contour width v_0. The values of h_g in the Hi $=$ 0.01 cases (C, F) are also smaller to allow for achievement of a tractable solution with very small Hi. Cross sections show the impermeable base elevation, water table elevation, and topographic elevation. Here zero elevation is the fixed topographic elevation boundary condition along the lower edge of the domain.

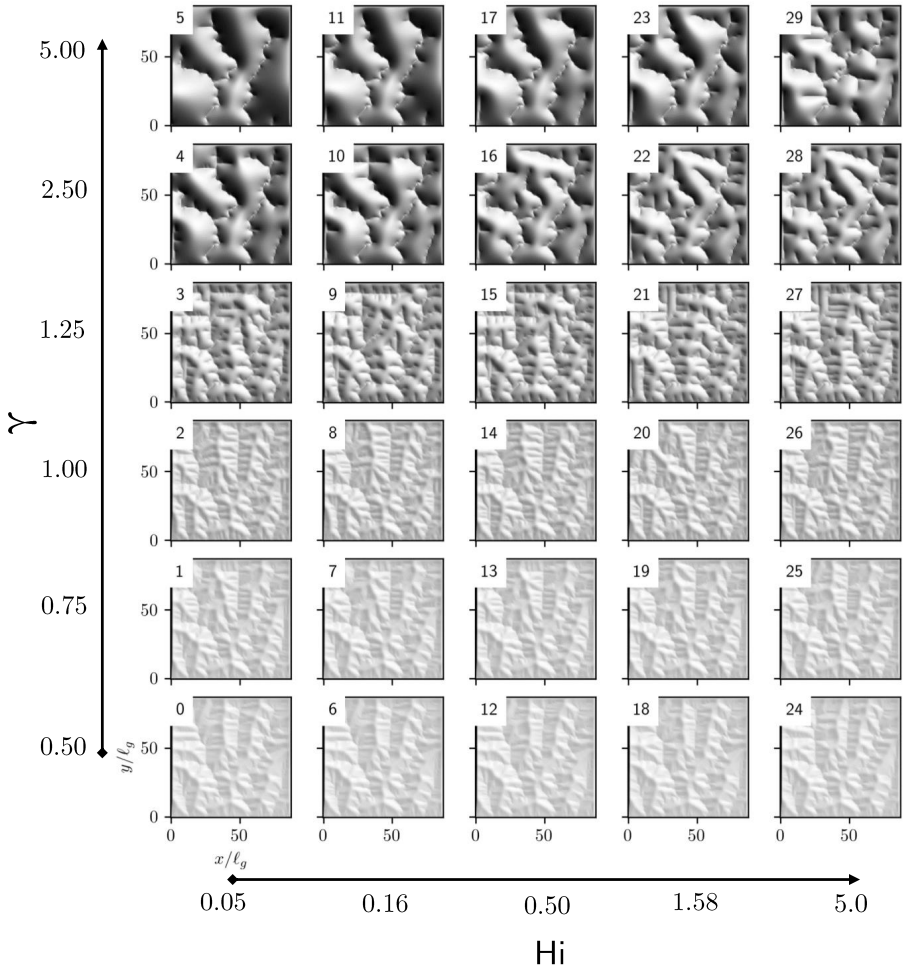

Figure 2. Hillshade plots of steady state elevation using the *DupuitLEM* model varying γ and Hi while α is held constant. Hi varies over two orders of magnitude on a geometric scale, while γ varies over one order of magnitude, further subdivided to show the transition that occurs at $\gamma = 1$. Low γ topography appears similar to *NoHyd* model results, and is less sensitive to varying Hi. Large γ results show broad hillslopes and slightly greater sensitivity to Hi.

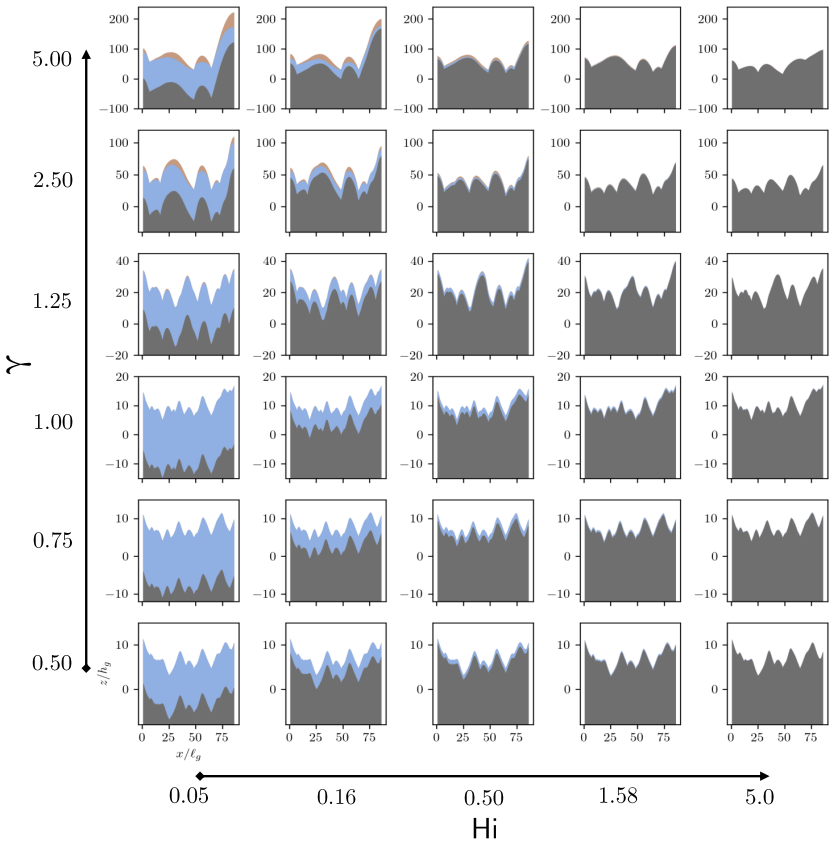

Figure 3. Cross section plots of *DupuitLEM* model results with varying γ and Hi corresponding to hillshades in 2. Cross sections are taken in the same fashion to 1, horizontally along the midpoint of the domain. Despite apparent similarities of the hillshades, there are prominent differences in the subsurface with varying Hi. Lower Hi cases will have deeper regolith, as this is dependent on the value of Hi. Noticeable depth to water table only becomes apparent at large values of γ.

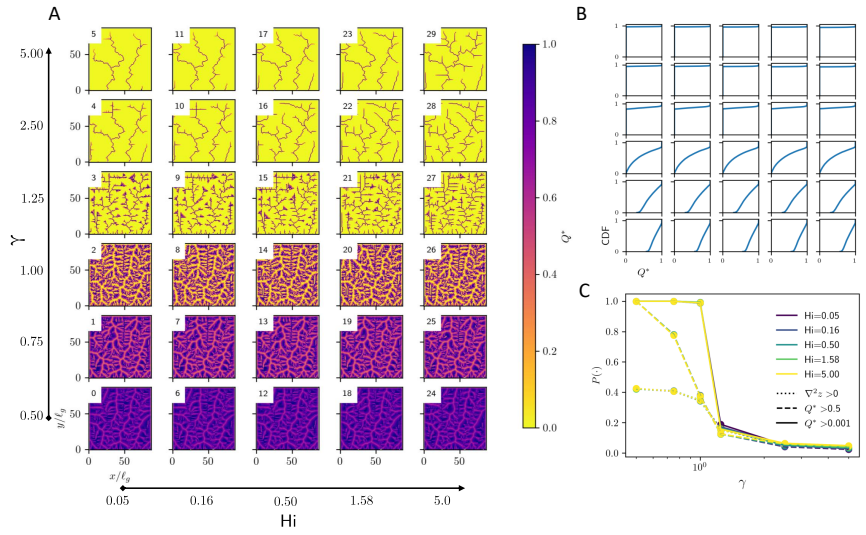

Figure 4. (A) Spatial patterns of Q^* from the *DupuitLEM* model varying γ and Hi while all other parameters are held constant. Results are similar across differences in Hi, but show significant differences with γ. All points in the landscape generate some runoff in the lowest *gamma* trials. (B) Cumulative distribution functions of Q^* with varying γ and Hi. Low γ trials show a range of Q^* values, with all areas contributing to some degree. High γ cases show most areas do not contribute runoff, with a small number where $Q^* \approx 1$. (C) Proportion of nodes contributing runoff at $Q^* > 0.5$, with varying γ (x-axis) and Hi (colors). Extent of areas contributing runoff is small for large Hi, and generally decreases with decreasing Hi.

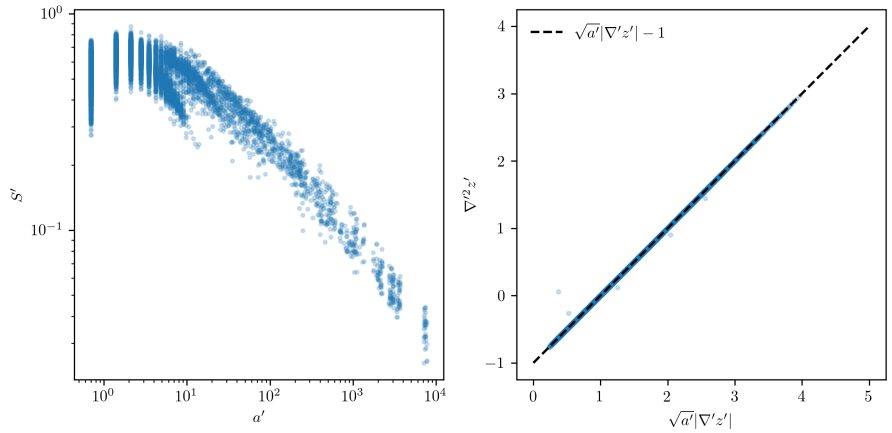

Figure 5. Dimensionless slope-area (left) and steepness-curvature plots (right) of steady state topography using the *NoHyd* model. Area per contour width is used in place of area in both plots to maintain consistency with model formulation. The steepness-curvature relationship observed in the data show a precise fit to the linear relationship predicted from theory (dotted line). Parameters selected are the same as Figure 1Ai.

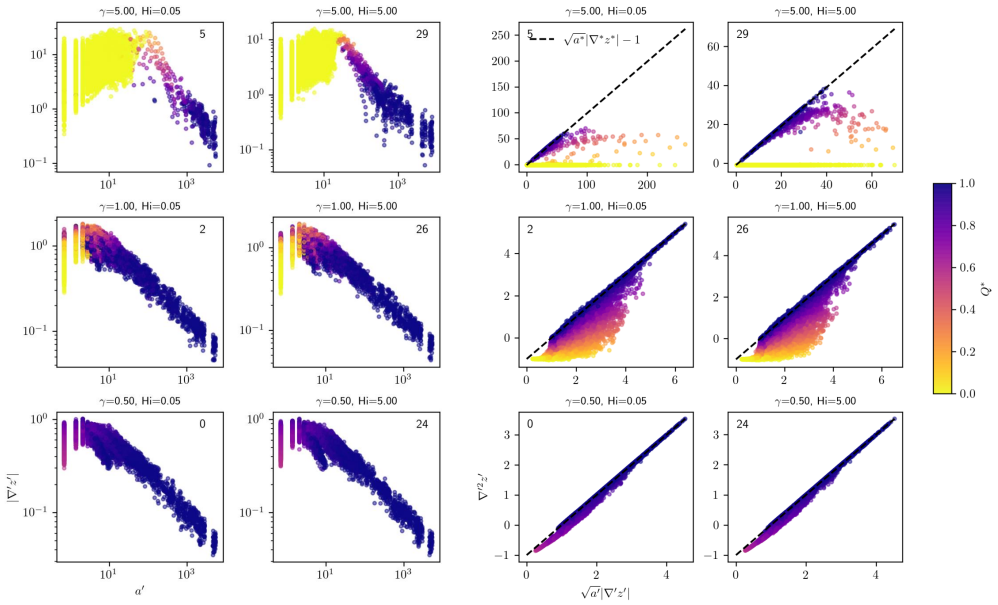

Figure 6. Dimensionless slope-area (left) and steepness-curvature (right) plots for selected model runs from Figure 2. See correlating numbers in the upper left corner. As in Figure 2, γ and Hi increase vertically and laterally from the bottom left respectively. Plots are colored by Q^* of the final topography. Axes scales are different between plots, showing that large γ cases obtain values of steepness and curvature far greater than the cases when γ is small.

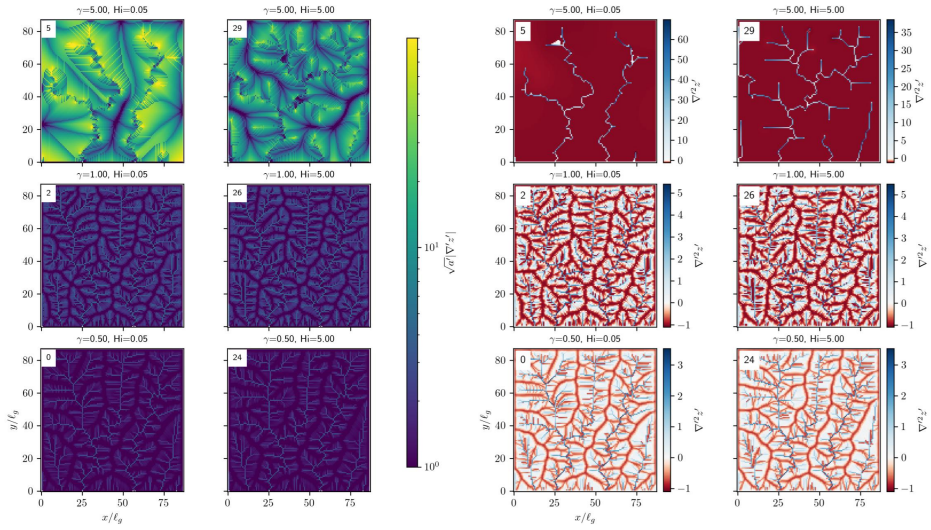

Figure 7. Planform view steepness and curvature for selected model runs, with run number corresponding to hillshades in figure 2. Spatial pattern of steepness appears to agree with channel network locations in the low γ cases, while in the high γ cases, it takes on large values in patterns that spiral away from ridges. Curvature is positive on ridges and negative in channels, with large areas of constant negative curvature in the large γ cases.

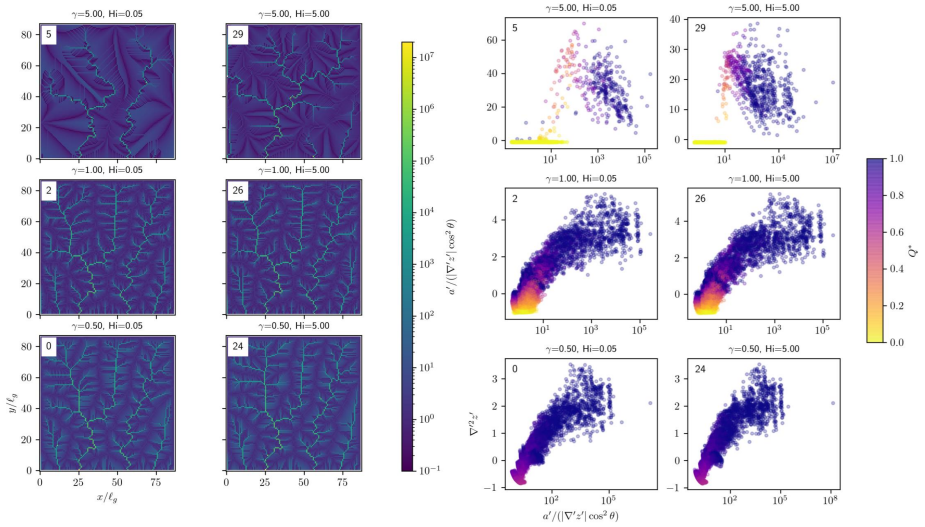

Figure 8. Planform view topographic index (left) and topographic index-curvature relationship for selected model runs, with run number corresponding to hillshades in figure 2

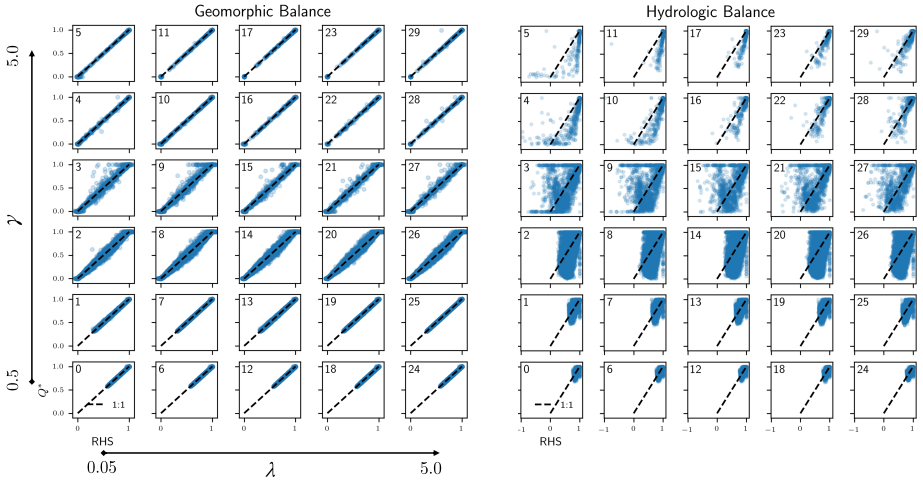

Figure 9. (A) Geomorphic balance from equation (62), plotting Q^* against the right hand side (RHS) of the equation. Subplots correspond to the same model runs as in 2. (B) Hydrologic balance from equation (70), plotting Q^* against the right hand side of the equation.

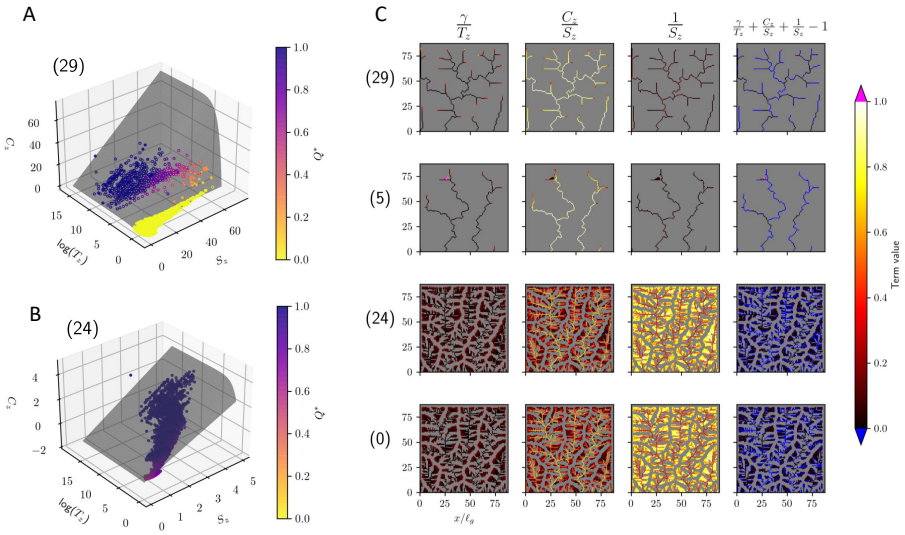

Figure 10. (A) Plot of the manifold (grey) defined in equation (73), with points plotted from model run (29), large Hi and large γ. The points in yellow are hillslope points, and lie on an approximately horizontal plane, not on the manifold. (B) Plot of the manifold defined in equation (73), with points plotted from model run (24), large Hi and small γ. (C) Map view of the terms of the hydromorphic balance in equation (73). Columns correspond to terms, with the final being the left hand side, which theory predicts to sum to zero. Rows are numbered with four different model runs with varying γ and Hi. Areas greyed out have $Q^* < 0.001$, thus representing hillslope points where the hydromorphic balance may not apply.

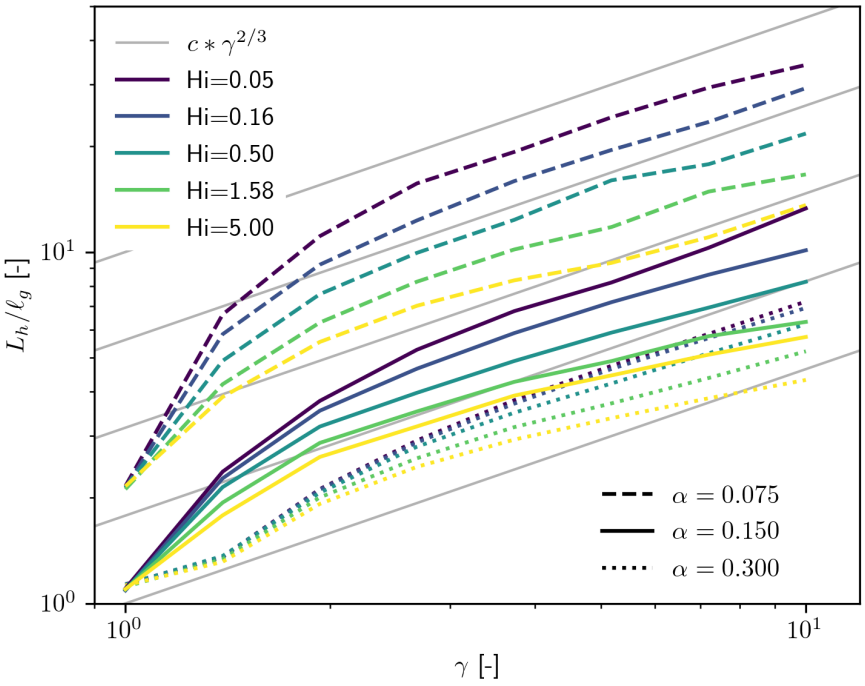

Figure 11. Hillslope length L_h increases with increasing γ. For a value of γ and α, L_h increases with decreasing Hi. Similarly, for a given value of γ and Hi, L_h increases with decreasing α. Gray lines with varying coefficients c show that the hillslope length scales approximately as $\gamma^{2/3}$ for $\gamma > 1$, which we derive from the hydromorphic balance.